# ARTICLE IN PRESS

Progress in Surface Science xxx (xxxx) xxx



Contents lists available at ScienceDirect

# Progress in Surface Science

journal homepage: www.elsevier.com/locate/progsurf



Review article

# Recent progress in probing atomic and molecular quantum coherence with scanning tunneling microscopy

Liya Bi $^{a,b}$ , Kangkai Liang $^{a,b}$ , Gregory Czap $^c$ , Hao Wang $^{d,e}$ , Kai Yang $^{d,e,*}$ , Shaowei Li $^{a,b,*}$ 

- <sup>a</sup> Department of Chemistry and Biochemistry, University of California, San Diego, La Jolla, CA 92093-0309, USA
- <sup>b</sup> Materials Science and Engineering Program, University of California, San Diego, La Jolla, CA 92093-0418, USA
- <sup>c</sup> IBM Research Division, Almaden Research Center, San Jose, CA 95120, USA
- d Beijing National Center for Condensed Matter Physics and Institute of Physics, Chinese Academy of Sciences, Beijing 100190, China
- <sup>e</sup> School of Physical Sciences, University of Chinese Academy of Sciences, Beijing 100190, China

#### ARTICLE INFO

Commissioning Editor: Dr. H. Petek

Keywords: Quantum coherence Scanning tunneling microscopy Molecular dynamics Electron spin resonance

#### ABSTRACT

Quantum coherent physics and chemistry concern the creation and manipulation of an excited-state manifold that contains the superposition and entanglement of multiple quantum levels. Electromagnetic waves such as light and microwave can be used to generate and probe different quantum coherent phenomena. The recent advances in scanning tunneling microscopy (STM) techniques including ultrafast laser coupled STM and electron spin resonance STM combine electromagnetic excitation with tunneling electron detection, bringing the investigation of quantum coherence down to the atomic and molecular level. Here, we survey the latest STM studies of different quantum coherent phenomena covering molecular vibration, electron transfer, surface plasmon resonance, phonon, spin oscillation, and electronic transition, and discuss the state and promise of characterizing and manipulating quantum coherence at the atomic or molecular scale.

#### 1. Introduction

Coherence, either classical or quantum mechanical, refers to the phenomena where wave-like amplitudes maintain a fixed phase relationship[1,2]. In the classical realm, coherent interference is often described with a deterministic position-time correlation function, such as the sinusoidal function used to outline the interference pattern in the double-slit experiment. In quantum mechanics, the probability amplitude of a state can be traced with wavefunctions. Quantum coherence arises from a series of wavefunctions that can maintain their entanglement and superposition[3,4]. Molecular-scale quantum coherence is ubiquitous in chemistry as it can be associated with nuclear motions[5–7], molecular orbitals[8–10], or periodic wave functions in molecular crystals[11,12]. It becomes especially enchanting in the context of light-matter interaction, where coherent electromagnetic fields, such as laser pulse, can create or modify molecular superposition states. This leads to a long-standing idea of coherent manipulation in chemistry: by precisely tuning the driving electromagnetic field, the population of a certain excited state can be artificially controlled, ultimately allowing us to steer the reaction pathway on demand[13–15].

https://doi.org/10.1016/j.progsurf.2022.100696

0079-6816/Published by Elsevier Ltd. This is an open access article under the CC BY-NC-ND license (http://creativecommons.org/licenses/by-nc-nd/4.0/).

Please cite this article as: Liya Bi, Progress in Surface Science, https://doi.org/10.1016/j.progsurf.2022.100696

<sup>\*</sup> Corresponding authors at: Department of Chemistry and Biochemistry, University of California, San Diego, La Jolla, CA 92093-0309, USA (S. Li) and Beijing National Center for Condensed Matter Physics and Institute of Physics, Chinese Academy of Sciences, Beijing 100190, China (K. Yang). E-mail addresses: kaiyang@iphy.ac.cn (K. Yang), shaoweili@ucsd.edu (S. Li).

The atomic- and molecular-scale quantum coherence is also of great interest and importance in quantum information science. A pair of entangled quantum states may serve as a qubit, which is the basic unit to apply quantum superposition principles in computational and cryptographic tasks that are impossible to accomplish by classical algorithms[16,17]. Meanwhile, coherent manipulation has the unique capability to prepare arbitrary superpositions of quantum states, a prerequisite for all quantum information processing protocols[18]. Many atomic or molecular systems that can maintain long-time coherence are natural candidates to realize different qubit-formation mechanisms, from altering the spin of an electron to leveraging the polarization of photons[19,20]. A major stumbling block all these systems share, however, is quantum decoherence: the loss of definite phase information from a binary coherent state into the environment over time, which can occur through various mechanisms from phonon scattering to exchange interactions with local impurities[21]. Atomic-scale understanding of the decoherence dynamics, and the precise characterization of the direct coupling between a qubit and its immediate chemical environment, are therefore essential in the design and application of atomic or molecular qubits.

Scanning tunneling microscopy (STM), invented nearly forty years ago was immediately recognized as a groundbreaking technology because of its atomic-scale spatial resolution[22]. Traditionally, STM could not provide adequate temporal information due to the limited electronic response time. The state-of-the-art time-resolved STM techniques which combine pulsed electromagnetic excitation with local tunneling electron detection have enabled the investigation of atomic and molecular dynamics that occur as fast as attosecond timescale[23–25]. For the first time, we have a technique that can simultaneously locate an atom or a molecule in real space and probe the time evolution of the probability density of its quantum states. This transforms an STM from a still camera that can only acquire high-definition photos into an ultrafast camcorder that can capture transient electronic and nuclear motions, making it an impactful approach to investigating atomic and molecular coherent phenomena. Here, we review the recent research on coherent processes such as molecular vibration[26–28], electron transport[29,30], plasmonic excitation[30], phonon[31,32], spin resonance [33,34], and electronic transition[35], revealed by different ultrafast STM techniques to highlight the progress and promise of space–time exploration of atomic- and molecular-scale quantum coherence.

#### 2. STM coupled with electromagnetic excitation

The combination of electromagnetic excitation and electron detection brings the strength of optical spectroscopy in the time and frequency domains together with the atomic-scale resolution of STM in real space and naturally becomes an ideal approach to visualizing atomic-scale quantum coherent phenomena (Fig. 1). Recently, several research groups have demonstrated the union of visible/ near-infrared (Vis/NIR) laser pulses with STM in an optical pump-probe scheme [28.30,32,35-40]. The advantage of using Vis/NIR photons is obvious: they cover a wide range of electronic and vibrational transitions of atoms and molecules and have been extensively applied in the studies of coherent phenomena in ensembles. In this scheme, paired laser pulses with a tunable delay time  $(\tau)$  are focused into the tunnel junction and the consequent localized current is detected. The former or pump pulse excites the sample and alters the transient signals associated with an excited state. Such transient signals, including photon-induced tunneling [30], surface photovoltage[37], the electron density of states[35], and photon-driven molecular transition rates[28], are characterized locally by measuring the tunneling current. The intensity of the signals evolves in time and is sequentially probed by the second laser pulse. By fitting the time-averaged transient signal as a function of  $\tau$ , one can therefore probe the dynamics of sample excited states at a time resolution limited by the laser pulse width. One major challenge arises from the weak photo-induced current signal compared with the relatively large background tunneling current, especially when it comes to the excitation from a single particle state in an atom or molecule. Specifically, even at 100 % quantum efficiency when each laser pulse excites an electron from a non-degenerated electronic orbital, only 0.16 pA tunneling current can be generated by a laser pulse train with a 1 MHz repetition rate. Therefore, a phase-sensitive method such as the lock-in technique is often essential to resolving the photo-included current in molecular studies [26,30,31,35–37,39–44]. Other approaches including the development of a high-sensitivity current pre-amplifier [26,27,45],

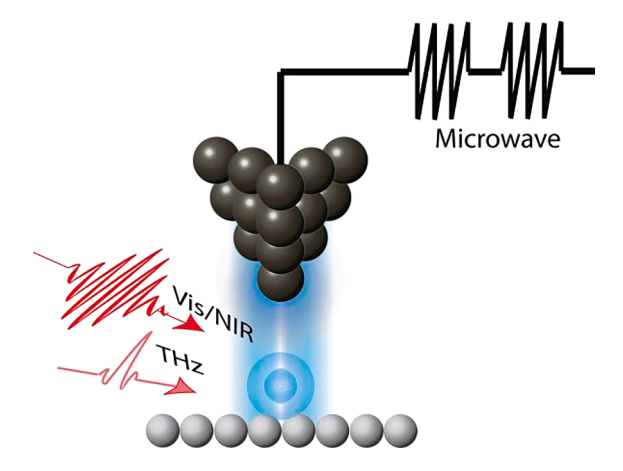


Fig. 1. Schematic of coupling STM with electromagnetic excitations in different wavelengths.

Progress in Surface Science xxx (xxxx) xxx

increasing the laser repetition rate [28], or measuring the laser induced molecular transition rate [27,28] are also adopted to improve the signal-to-noise ratio. Since the desired electronic transition of an atom or molecule only consumes a small portion of the laser energy, the rest of the pulse dissipates into heat. This poses another challenge in maintaining atomic-scale mechanical stability in the STM junction under laser illumination. The tip expands (contracts) in response to the presence (absence) of the laser pulses. Since the tunneling current is very sensitive to the tip-sample separation, even a small fluctuation of the laser power can cause changes in the length of the STM tip which interferes with the STM measurements. It becomes especially problematic when chopper or power modulation is applied to the laser beam to perform lock-in measurements. Thus, a low-energy and power-stabilized laser is necessary for suppressing signal artifacts from thermal-mechanical fluctuations in the tunnel junction. Several methods have been developed to avoid the thermally induced mechanical fluctuation of the STM junction. Firstly, instead of chopping the probe pulses, modulation to  $\tau$ [37], pulse duration[39], frequency of carrier wave[35,39], or polarization of electric field[35,39] was applied for lock-in detection to avoid a dramatic change of thermal load at the STM junction, Secondly, the increase of laser repetition rate to the GHz scale can reduce the energy of a single pulse without hindering the yield of the signal [28]. Thirdly, lenses [36] or parabolic mirrors [30] in proximity to the STM junction were used to increase the numerical aperture of the optical pathway to tightly focus the laser beam. Finally, with low-energy (~2.5 nJ) and high-repetition-rate (80 MHz) ultrashort (<6 fs) laser pulses, Garg et al. showed that the thermal fluctuation at the tunnel junction is negligible (<1 pm) if the probe pulses are chopped at a frequency higher than 1 kHz [30,39], though others also reported that thermal perturbation may remain problematic with similar modulation frequency [36,46,47].

The recent developments in terahertz (THz) techniques also provide an optimal solution to the thermal fluctuation of the STM junction. When used as the probe pulse in the pump–probe scheme, the THz photon energy is low enough to avoid inducing thermal expansion of the STM tip. Instead of interacting with the sample through photon absorption, the THz pulse generates a transient electric field to the tip-sample junction which induces a rectification tunneling current[26,27,29,31,41–44,48–52]. Owing to the local field enhancement effect, the THz field is strongly confined at the atomically sharp STM tip apex. Since the tip-sample separation is usually several angstroms, the quasistatic THz-induced bias is strong enough to modify the tunneling barrier and hence introduce ultrafast electron tunneling. Due to the nonlinearity of the I-V curve, the time-averaged THz-induced tunneling current is non-zero and thus can be read out by the current amplifier using the lock-in technique[42,53]. Another important advantage of the THz pulse is the stability of its carrier-envelope phase (CEP)[53–55]. Since the phase of the driving laser pulse is correlated with the probability amplitude of the superposition states it excites, a stable CEP is especially critical in the investigation of coherent phenomena. The THz pulses can be generated with the tilt-pulse-front optical rectification[56–58], spintronic emitter[59,60], or plasmonic photoconductive antenna[61,62], all are difference frequency generation processes that automatically yield a locked CEP. This avoids the complicated and often expensive approaches commonly applied to achieve a stable CEP in the Vis/NIR range[63–65].

At an even longer wavelength scale, the combination of radiofrequency (RF) excitation with spin-polarized STM further expands the study of electron spin resonance (ESR) to the single atom and molecule level[33,34,66-68]. Different from the Vis/NIR or THz coupled STM where the electromagnetic excitation is provided through a free-space laser, the RF signal in an ESR-STM is generated using a microwave generator and transmitted to the tunneling junction through coaxial cables. To compensate for the energy loss through the cabling, the RF source power is typically varied according to the frequency-dependent transfer function to generate a constant-amplitude RF field at the tunnel junction [69]. In an ESR-STM measurement, a magnetic tip is positioned on top of a single magnetic atom or molecule. An RF electric field (typically ~ 20–30 GHz) is then applied across the STM tunnel junction to drive the spin transitions between spin-up and spin-down states, which are separated by the Zeeman energy due to an external magnetic field. While the primary mechanism of ESR-STM remains under debate in the literature [70-74], the most commonly assumed and experimentally supported one remains the magnetic interaction modulation mechanism[70,71]. In this scenario, the RF electric field induces a piezoelectric displacement of the surface atom, which results in a time-varying perpendicular magnetic field sensed by the surface atom as it mechanically displaces toward and away from the magnetic tip[71,75,76]. The initialization of the surface spins is due to the thermal polarization in an applied magnetic field as well as the spin torque from the spin-polarized tunneling current. The detection of the ESR signal relies on the change of tunneling magnetoresistance of the tunnel junction as the spin is driven away from its initial spin population in an applied RF field [75,77]. The spin-polarized STM tip plays an important role in the ESR-STM experiment. A magnetic tip with a canted magnetic moment with respect to the external field provides both the oscillating magnetic field to drive ESR and also spin polarization to detect the change of time-average spin populations by tunneling magnetoresistance [71]. In addition, the magnitude of the tip field can be adjusted by changing the tip-surface distance, covering a range from 1 mT to 10 T, which offers a local knob to tune the surface spin states [78,79]. In general, the experiment needs to be performed at an extremely low temperature (~1 K) and under a strong magnetic field (>1 T) so that the energy separation between the spin states is comparable to or larger than the Boltzmann energy. Nonetheless, the recent application of a specially designed bowtie antenna located  $\sim 1.8$  cm from the tunnel junction is shown to effectively enhance the RF amplitude in the higher frequency range ( $\sim 100$  GHz), which would confer major benefits in experiments run at 4-5 K[80]. The spin dynamics information, such as the energy relaxation time  $T_1$  and dephasing time T<sub>2</sub>, can be probed by an electronic pump–probe measurement using incoherent[81–84] or coherent voltage pulses[33,34,75]. Since ESR-STM is essentially an all-electronic approach, the time resolution is limited by the electronic response time to the nanosecond timescale, which is high enough to study spin coherence and dynamics for quantum sensing and simulating quantum magnetism but remains too low to resolve the relatively fast processes related to spin-orbit or spin-phonon coupling [85,86].

# 3. Recent STM studies of quantum coherence

#### 3.1. Vibration of single molecules

An electromagnetic perturbation, such as a short laser pulse, can induce the coherent oscillatory motion of atoms within molecules, establishing molecular vibrational coherence[7]. These vibrational states can often be approximated as a semiclassical harmonic oscillator whose probability density exhibits a sinusoidal oscillation in time, which can either directly affect electron tunneling or couple with a molecular reaction coordinate, both detectable by STM with sub-Angstrom spatial resolution. Depending on the symmetry, the vibrational dynamics can be traced by various ultrafast signals. For example, the bouncing vibration of a molecule on a surface directly alters the distance between the molecule and the tip which changes the intensity of the tunneling current[26]. The

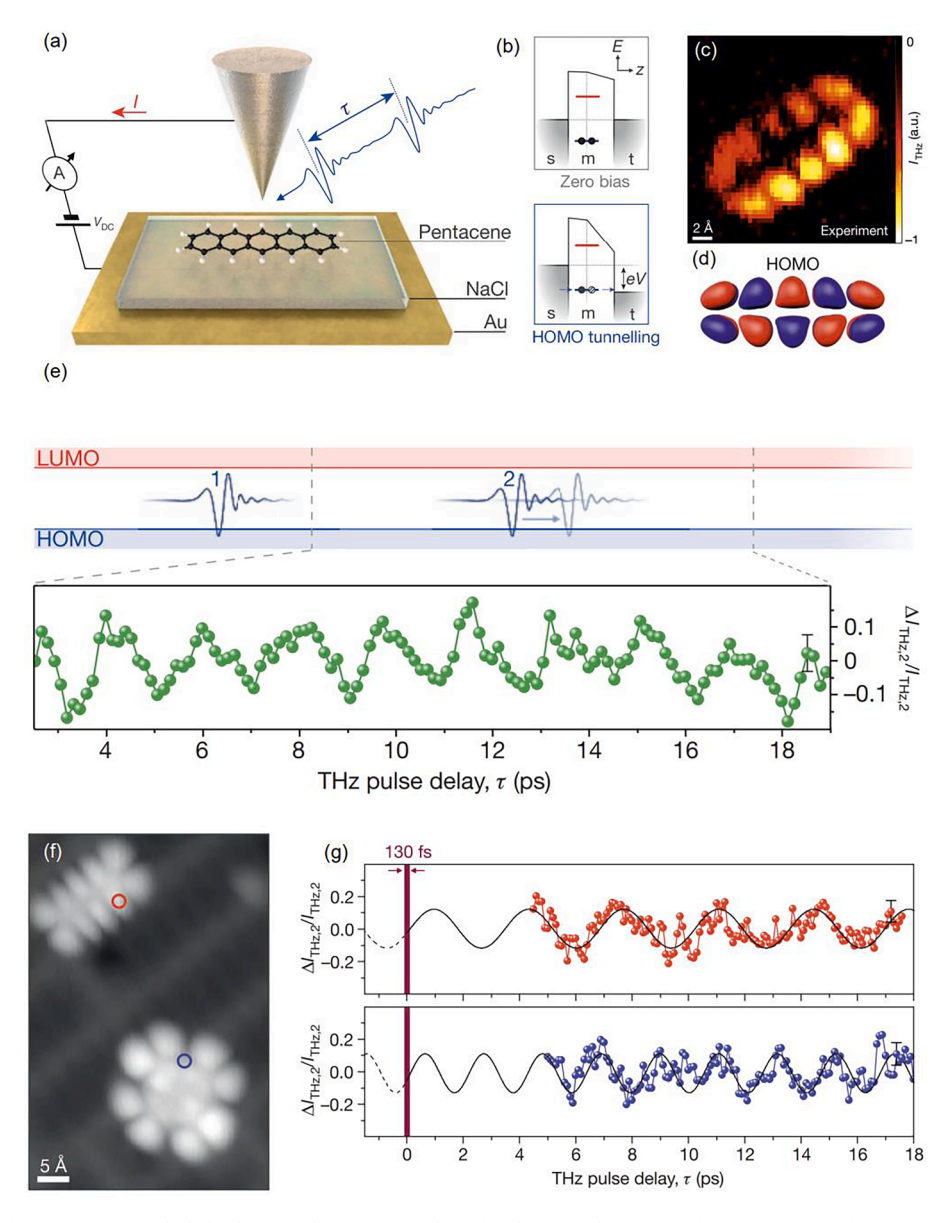


Fig. 2. STM visualization of THz included coherent vibration of single molecules. (a) Schematic of the THz pump–probe measurement on a surface-adsorbed pentacene molecule. (b) THz-induced tunneling from HOMO of molecule to tip. V represents the ultrafast THz-induced voltage pulse. s, m and t stand for sample, molecule and tip respectively. (c) Spatial mapping of the THz-induced tunneling current over a pentacene molecule. (d) DFT result of HOMO contours of a free pentacene. (e) Pump-probe measurement over a pentacene shows oscillating current signal as a function of delay time  $\tau$ . (f) Topographic image of a pentacene (top left) and a CuPc (bottom right) on NaCl/Au(110) without Au(110) missing-row reconstruction. (g) THz pump–probe scan on pentacene (top) and CuPc (bottom). The positions of the tip during measurement are indicated by the circles of corresponding colors in (f). Reprinted and adapted with permission from Ref. [26]. Copyright 2016 Springer Nature.

frustrated rotation or bending vibration may modulate the rate of a molecular structural transition[27,28]. For a single-molecule study, the molecule needs to relax to an equilibrium ground state during the pulse interval, so that the pump pulse always interacts with the same molecular initial state. The coupling between the vibrational degree of freedom and the environment (the "bath" degrees of freedom) often leads to a comparatively fast dephasing and relaxation typically in picoseconds. Recently, several research groups reported the observation of vibrational coherence of individual molecules using ultrafast laser coupled STM[26–28].

By coupling the femtosecond CEP-locked single-cycle THz pulses with STM, the groundbreaking experiment by Cocker *et al.* successfully unveiled the coherent vertical vibration of a single pentacene molecule on a NaCl/Au(110) substrate (Fig. 2a)[26]. In this experiment, the THz pulse generates a transient voltage pulse at the tunneling junction which can induce electron tunneling from the highest occupied molecular orbital (HOMO) of pentacene to the tip (Fig. 2b). The temporary ionization of the molecule is confirmed by the spatially resolved mapping of the THz-induced tunneling current at nearly zero DC bias voltage, which reveals the spatial distribution of the HOMO that otherwise can only be accessible at the resonant bias (Fig. 2c-d). The time-resolved pump-probe experiment is performed on the molecule with sequential equivalent THz pulses separated by a delay time  $\tau$ . The THz-induced tunneling current generated by the probe pulse exhibits a  $\sim$  0.5 THz oscillation, assigned as the out-of-plane vibrational motion of the molecule (Fig. 2e). The vibrational excitation was attributed to the result of the transitory change of the Coulomb and van der Waals forces on the molecule upon ionization. Furthermore, a smaller oscillation frequency,  $\sim$ 0.3 THz, is measured on the pentacene on NaCl/Au (110) without an underneath missing-row reconstruction, which showcases the modification of molecular vibrational dynamics by adjusting the weak van der Waals interaction with the underlying substrate. A similar vibrational coherence ( $\sim$ 0.5 THz) is also reported on copper phthalocyanine under the same experimental conditions (Fig. 2f-g).

In follow-up work, Peller *et al.* further associated the vibrational coherence of a molecule with conformational changes and demonstrated the connection between the CEP of the driving THz pulse and the phase of the vibrational oscillation[27]. Here, the

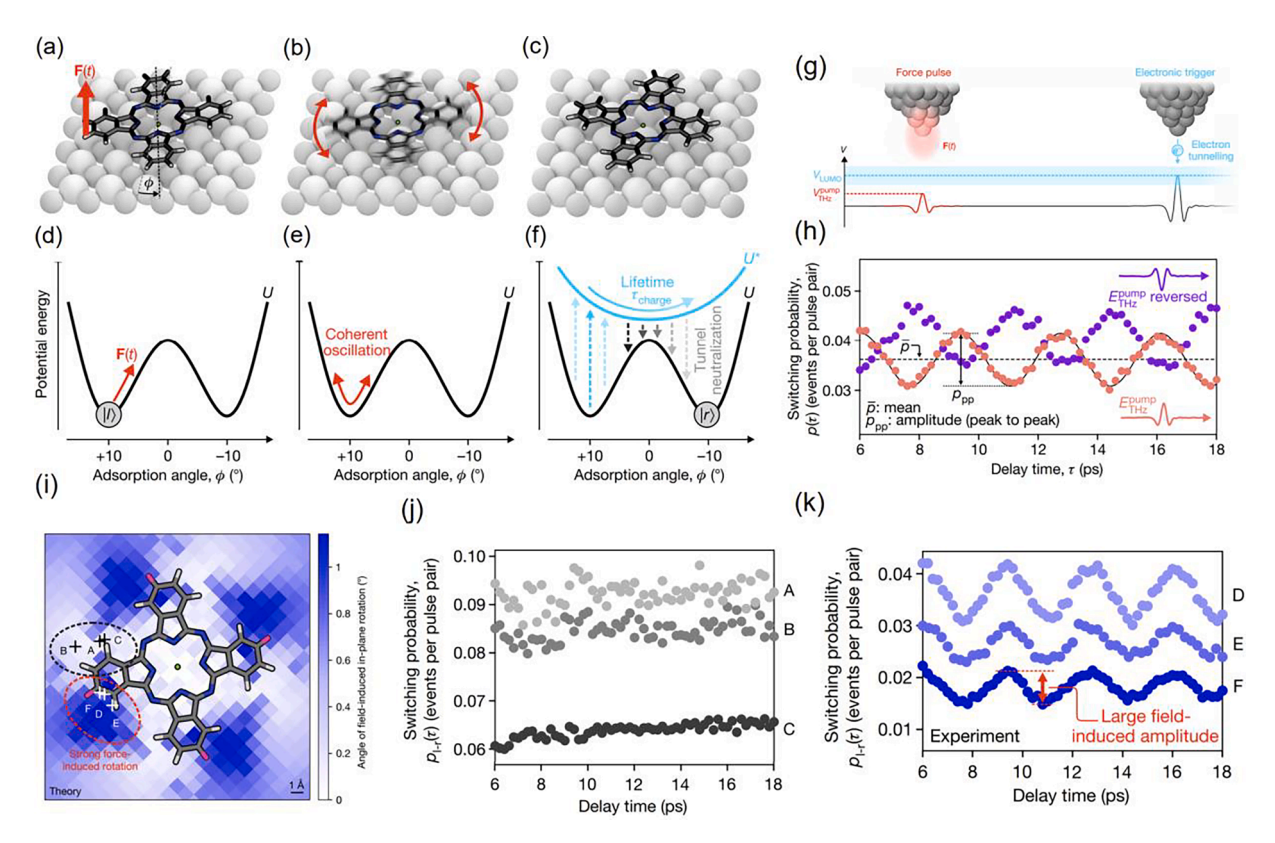


Fig. 3. Single-molecule switch mediated by the coherent in-plane frustrated rotation. (a)-(c) Schematic of the switching of MgPc on NaCl/Cu(111) from conformational state |1> to |r> mediated by the localized force, F(t), induced frustrated in-plane rotation. (d)-(f) The potential energy profile of MgPc as a function of the adsorption angle and the evolution of the MgPc during the switching process. The blue parabolic curve in (f) is the energy profile of the temporally negatively charged MgPc before tunneling into one of the two stable states. (g) The THz pump-probe scheme where the weak pump pulse only exerts a local force on the molecule to induce hindered rotation while the strong probe pump triggers electron tunneling into the LUMO of MgPc to initiate the switching and to enable tunneling current detection. (h) The switching probability as a function of delay time. The purple and pink data points were collected with reversed pump pulse. (i) Simulated spatial distribution of the amplitude of in-plane rotation locally triggered by the THz pulses. The MgPc with selected hydrogen atoms painted in pink is overlaid. (j) Switching probability over the positions indicated in (i) as a function of delay time, exhibiting negligible modulation. (k) Switching probability over the positions indicated in (i) as a function of delay time, demonstrating large field-induced modulation. Reprinted with permission from Ref. [27]. Copyright 2020 Springer Nature. (For interpretation of the references to colour in this figure legend, the reader is referred to the web version of this article.)

transient voltage generated by a relatively strong THz pulse can induce the temporary ionization of a bistable magnesium phthalocyanine (MgPc) on the NaCl/Cu(111) surface by electron tunneling into its lowest unoccupied molecular orbital (LUMO). The molecular anion then quantum mechanically relaxes from a parabolic potential landscape to one of the two stable adsorption geometries, resulting in molecular conformational switching (Fig. 3a-f). The spatial variation of the switching probability measured across the molecule strongly correlates with the simulated tunneling probability into the LUMO of MgPc. When the molecule interacts with a relatively weak THz pulse, the transient field is not enough to induce switching of MgPc but can trigger its frustrated in-plane rotation (Fig. 3a-b). The dynamical correlation between the coherent molecular vibration and the molecular switching can therefore be probed using a weak pump pulse and a strong probe pulse separated by a tunable delay time  $\tau$  (Fig. 3g). This mechanism is validated by the  $\sim$  0.3 THz oscillatory patterns in the measured switching probability as a function of  $\tau$  and further corroborated by the 180 phase shift of the observed oscillation when the polarity of the pump pulse is reversed (Fig. 3h). It is interesting to note that clear oscillations can be observed with either strong or weak pump pulses, indicating that the vibrational excitation could be independent of molecular ionization. Since the THz pulse mainly introduces an out-of-plane electric field, the excitation of the hindered rotation was rationalized as the result of the perturbation to the interaction between the four end hydrogen atoms on MgPc and the underlying chlorine and sodium ions, which defines the double-well surface adsorption potential. This hypothesis was supported by the much larger modulation to the switching probability observed when the tip is parked near those hydrogen atoms (Fig. 3i-k).

Besides THz radiation, NIR laser pulses can also trigger coherent molecular vibration through, for example, the impulsive stimulated Raman scattering (SRS) process. Li *et al.* observed the coherent vibration-driven conformational transitions of a single pyrrolidine molecule on Cu(001) by coupling broadband ( $\sim$ 46 meV energy spread) NIR femtosecond laser pulses with an STM (Fig. 4a)[28]. In their experiment, the surface-adsorbed pyrrolidine molecules can switch between two conformational states (named I and II) when

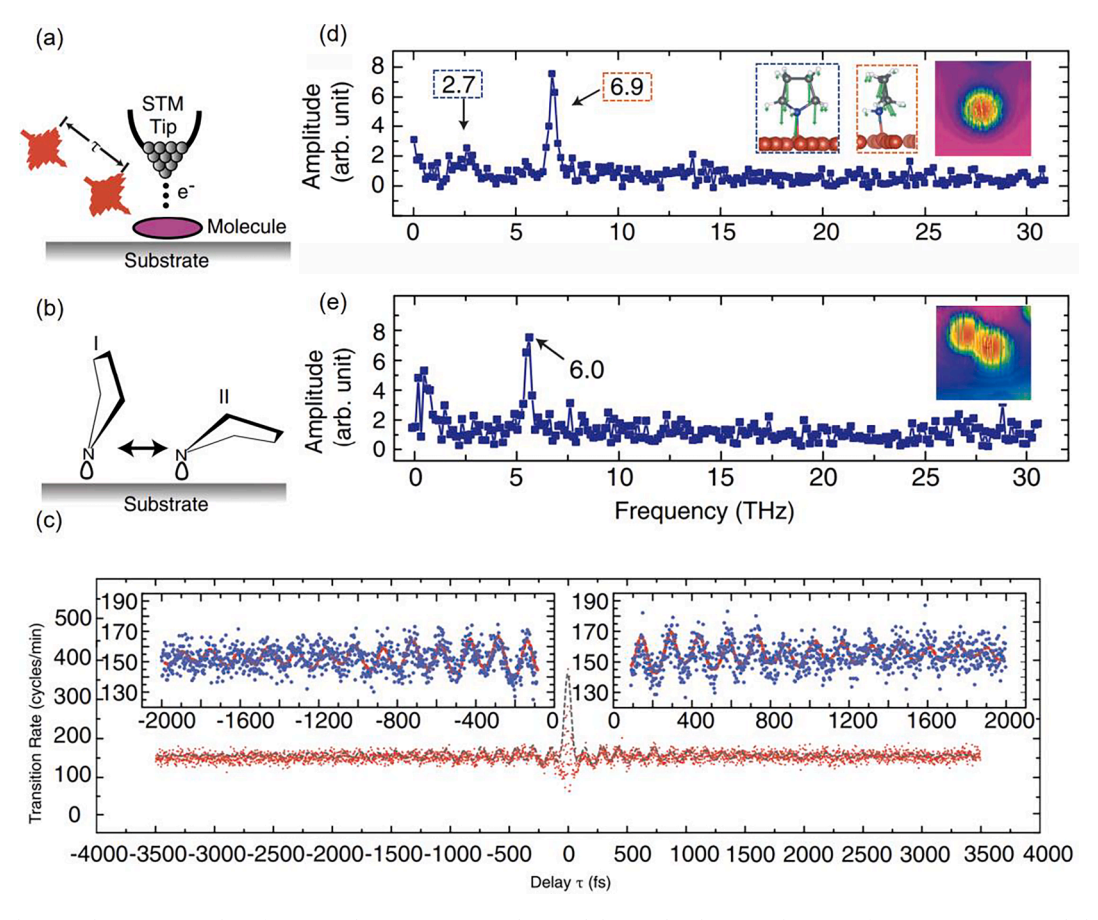
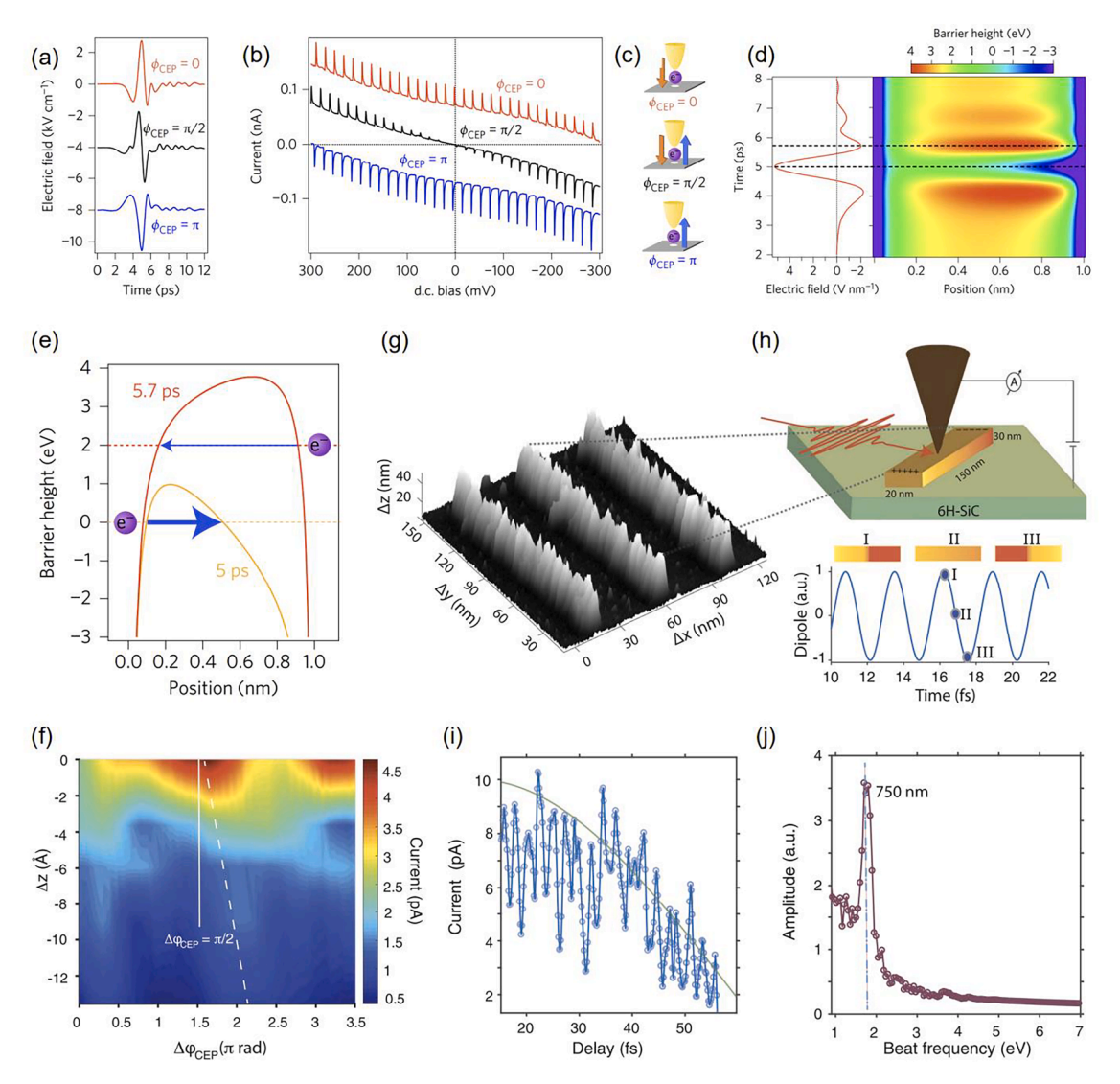


Fig. 4. Coherent vibration assisted conformational transitions in single pyrrolidine molecules. (a) Schematic of an STM junction coupled with NIR pump–probe pulses. (b) Two interchangeable conformational states I and II of pyrrolidine on Cu(001). (c) Delay scans with identical NIR pulses over the center of a pyrrolidine. The transition rate is defined as I-II-I cycles per minute. The red and bules dots are experimental data which are fitted (black and red dashed lines) with a function of three components: two exponentially decaying sinusoidal functions, a constant and a Gaussian function. (d) Fourier transform of the data in (c) shows a dominant peak at  $6.9 \pm 0.2$ THz and a weak peak at  $2.7 \pm 0.3$ THz. The left and middle insets are the DFT-calculated vibrational modes and are assigned to the weak and dominant peaks respectively. The right inset is the topographic image of the pyrrolidine over which the data in (c) were taken. (e) Fourier transform of the delay scan taken over the center of a pyrroline dimer which is shown in the inset. Reprinted and adapted with permission from Ref. [28]. Copyright 2017 American Physical Society. (For interpretation of the references to colour in this figure legend, the reader is referred to the web version of this article.)

excited by either tunneling electrons or photons (Fig. 4b). The switching events are recorded by monitoring the sudden change in the tunneling gap  $\triangle$ z. Under femtosecond laser illumination, the transition rate (defined as I-II-I cycles per minute) significantly increases. The pump–probe measurement of transition rate with a pair of identical laser pulses exhibits a remarkable  $\sim 6.9$  THz oscillatory feature with a weak  $\sim 2.7$  THz modulation, assigned as the bending vibrational mode ( $\sim$ 27.24 meV) and the bouncing vibrational mode ( $\sim$ 11.85 meV) respectively by comparing with DFT calculations (Fig. 4c-d). A  $\sim 1.3$  ps decay time is extracted from fitting the data with two exponentially decaying sinusoidal functions. Since the molecule doesn't have well-defined electronic states on the metal surface, photon absorption through the Frank-Condon transition is unlikely. The authors attributed the vibrational excitation to SRS where the energy spread of the pump NIR pulse covers both the bending and bouncing vibrational modes. The experiment also reveals that the coherent dynamics changes with another molecule in proximity. The dominant oscillation measured over a pyrrolidine in a



**Fig. 5.** Coherent manipulation of electron transfer and observation of LSPRs at the STM junction. (a) Electric-field profiles of THz pulses with different CEPs. (b) CEP-dependent tunneling current as a function of DC bias. (c) Illustration of CEP-dependent direction of electron tunneling. (d) Simulated ultrafast evolution of tunneling barrier across the junction, right panel, under the illumination of the THz pulses, left panel. (e) The barrier height as a function of tunneling gap at different time, as indicated by the black dashed lines in (d). The arrow lines show the tunneling direction and the thicker the line, the higher the tunneling probability. (f) Modulation of tunneling current at different tunneling gap by varying the CEP of the ultrashort NIR laser. The white dashed line shows the shift of current maxima when the tunneling gap changes. (g) Topographic image of three Au nanorods on *n*-doped 6H-SiC. (h) Top panel: Schematic of the Au nanorod excited by NIR laser pulses. Bottom panel: Illustration of the surface plasmon oscillation in Au nanorod in both time and spatial domain. (i) The blue curve is the temporal evolution of the laser-induced tunneling current over the Au nanorod and the green one shows the exponential decay of the current signal. (j) Fourier transform of the data in (i). Reprinted with permission from Ref. [29] Copyright 2016 Springer Nature and Ref. [30] Copyright 2020 American Association for the Advancement of Science. (For interpretation of the references to colour in this figure legend, the reader is referred to the web version of this article.)

dimer decreases to  $\sim 6.0$  THz in frequency and decays within 1 ps, highlighting that even the molecular-scale influence of the local chemical environment can alter the coherent dynamics (Fig. 4e).

## 3.2. Electron transfer and collective oscillation

The dynamical motions of electrons govern many physical, chemical, and biological processes. Manipulation of electron motions can make profound impacts on both macroscopic and microscopic levels from ps-scale electron tunneling in photosynthetic reaction centers[87] to ms-scale electron transfer in centimeter-long DNAs[88]. The recent advances in ultrafast laser technology have made it possible to generate and control the CEP of laser pulses with high accuracy. Using few-cycle CEP-tunable laser pulses, several research teams have demonstrated the manipulation of electron motions at the STM junction[29,30].

In 2016, Yoshioka *et al.* showcased the coherent manipulation over directional electron tunneling at the STM junction with subpicosecond temporal resolution[29]. They observed the change of tunneling current polarities in response to the CEP of the THz pulses. In this study, the STM tip over a highly oriented pyrolytic graphite surface is shined with single-cycle THz pulses of 3 different CEPs ( $\phi_{CEP} = 0, \pi/2$ , and  $\pi$ , respectively) (Fig. 5a). The THz pulses with  $\phi_{CEP} = 0$  modulate the tunnel barrier in a sub-picosecond timescale (Fig. 5d-e) and induce the transient electron tunneling from tip to sample. When  $\phi_{CEP}$  is shifted by  $\pi$ , electrons tunnel in the opposite direction. In the case of  $\phi_{CEP} = \pi/2$ , the direction of the THz-induced electron tunneling depends strongly on the DC bias: electrons undergo tunneling from the tip to the sample under a positive bias while in the opposite direction under a negative bias (Fig. 5b-c). This study demonstrates the control of the electron tunneling direction with CEP.

More recently, Garg and Kern took one step further and pushed coherent control over the tunneling electrons to the attosecond timescale[30]. In this experiment, an Au surface is illuminated by ultrashort (<6 fs) NIR (810 nm center wavelength) laser pulses with continuously adjustable CEP. The CEP corresponds to the maximum tunneling current shifts by  $\pi/2$  as the tip approaches the surface by 0.9 nm, which was attributed to the decrease of the traveling time of the electron in the junction by  $\sim$  600 as, 1/8 of the pulse width of the two-cycle laser used in the experiment (Fig. 5f). In addition to the single-electron motion, they also visualized the femtosecond scale decay dynamics of the collective electron oscillations in the  $150 \times 20 \times 30$  nm Au nanorods grown on atomically flat n-doped 6H-SiC (Fig. 5g-j). In the pump–probe measurement with identical broadband NIR pulses, the field-driven tunneling current oscillates at a wavelength of 750 nm, which was assigned to the longitudinal mode of the localized surface plasmon resonances (LSPRs) in the Au nanorods with an aspect ratio (length/width) of  $\sim$  8. A decay time of  $\sim$  40 fs is extracted from fitting the current and was attributed to the fast electron scattering process.

#### 3.3. Coherent phonon

Besides the efforts focused on the nuclear motions of molecular adsorbates, the recent THz-STM experiments have also explored the collective movement of atoms in solid-statete materials. Sheng  $\it et al.$  have shown that THz pulses incident on the tunnel junction can induce ultrafast Coulomb forces in thin Au films grown on Mica, allowing the creation of coherent acoustic phonon wave packets[31]. These coherent phonons (CPs) propagate through the film, reflecting several times at the vacuum and Mica interfaces at either side of the Au thin film which results in periodic mechanical breathing of the Au surface atoms on the scale of picometers. These mechanical oscillations of the surface can be detected as a transient modulation of the tunneling barrier when probed by picosecond pump–probe spectroscopy. The frequency of the CP surface oscillation is found to match the calculated acoustic phonon frequency of the thin film at its measured thickness and shifts dramatically from  $\sim 10$  GHz to  $\sim 260$  GHz as the film thickness is reduced from  $\sim 150$  nm to  $\sim 6.5$  nm. Further anomalous surface oscillations at other frequencies appear in the pump–probe spectra and are found to be dependent on the local positions of the tip, strongly hinting at the possibility of characterizing phonon scattering from local defects and surface features at the nanoscale. These results establish that the observed periodic oscillation of the tunneling barrier is indeed a property of the gold film and further points to new experiments in space–time resolved coherent phonon experiments. Since CPs can transiently modulate material properties, excite spin waves, and have long propagation lengths with low loss, the ability of THz-STM to study this phenomenon in detail constitutes an important and timely advancement.

In a more recent work, Liu *et al.* reported the NIR pulses excited CPs of the ZnO thin films in a plasmonic tunnel junction [32]. In the experiment, the NIR pulses are confined to the nanoscale by the nanoscopically sharp Ag tip and Ag(111) surface, producing picoampere-scale photoexcited current  $I_{photo}$  via LSP excitation. Instead of measuring in the tunneling regime, they detected the  $I_{photo}$  after lifting the tip well above the tunneling setpoint where the contribution from the DC tunneling current is negligible. When collecting the  $I_{photo}$  over a 3-monolayer ZnO thin film on Ag(111), a negative bias is added so that the photo-assisted tunneling from the ZnO to the tip dominates while that in the other direction is suppressed. As revealed by the pump–probe measurement, the  $I_{photo}$  exhibits oscillation damping in several picoseconds, which was assigned to CP modes after comparing its Fourier transform spectrum with the tip-enhanced Raman spectrum acquired over the same location. Since the  $I_{photo}$  mainly sources from the resonant electronic transition from the interface state to the conduction band edge of the ZnO on Ag(111), the authors rationalized that the CPs modulate the transition probability between the interface state and the conduction band edge and hence results in the oscillatory  $I_{photo}$ . It was further shown that the CP modes vary on the nanoscale, again demonstrating the unique capability of laser-coupled STM on probing the local coherence dynamics.

#### 3.4. Electron spin resonance in single atoms and molecules

Individual atomic and molecular spins on surfaces provide a versatile platform for future spintronic and quantum computing applications[77,89,90]. To detect and control the quantum states of surface spins with high precision, ESR-STM has been applied to probe the spin states of magnetic atoms and molecules with ultra-high energy resolution[66,75–78,91–94] and to realize coherent spin manipulation of single magnetic atoms and molecules on surfaces[33,34].

Using a homemade low-temperature (1.2 K) STM, Yang  $et\,al.$  realized the coherent spin manipulation of single Ti atoms by a pulsed-ESR technique[33]. Fig. 6a shows the schematic of the experimental setup. Spin-1/2 Ti atoms were placed on the surface of a bilayer MgO film grown on Ag(001), and a series of RF pulses at the resonant frequency were then applied to induce Rabi oscillations between the spin-up  $|\uparrow\rangle$ , and spin-down  $|\downarrow\rangle$  states. Here, the resonant frequency of the Ti atom is determined by measuring its continuous-wave ESR (CW-ESR) spectrum where the RF frequency was swept and the external field was kept constant at about 0.8 T. During the RF pulses, the Ti was coherently rotated between the  $|\uparrow\rangle$  and  $|\downarrow\rangle$ , giving rise to oscillatory tunneling magnetoresistance with increasing time durations of the RF pulses (Fig. 6b). The Rabi oscillation signal in Fig. 6b was obtained by using a homodyne detection scheme where the time-averaged current due to the RF voltage was measured, giving rise to a better signal-to-noise ratio than measurements using DC pulses[33]. The Rabi frequency increases monotonically with RF amplitude and exhibits an exponential dependence on the tip-atom distance at constant DC and RF voltages. The exponential dependence is an important feature of the exchange-field-driven ESR mechanism as mentioned in Section 2. In addition, the coherence time of the Ti spin on MgO can be obtained from the decay constant of the Rabi oscillations, which is about 40 ns.

To improve the spin coherence time, the Ramsey fringes and spin echoes of Ti spins were measured[33]. The Ramsey measurement consists of two  $\pi/2$  pulses separated by a time delay, where  $\pi$  represents a spin flip between  $|\uparrow\rangle$  and  $|\downarrow\rangle$ . Since the RF frequency was detuned, an interference fringes signal can be measured due to a phase accumulation between the two spin components with increasing time delay. The decoherence time corresponding to the Ramsey fringes is about 40 ns, which is almost the same as the value obtained from the Rabi oscillations. It is concluded that the decoherence due to the RF current and the slight variation of the Rabi oscillation frequency resulting from the change of tip-atom distance is negligible[33]. The spin coherence time was extended by using a Hahnecho pulse sequence with an additional  $\pi$  pulse inserted between the two  $\pi/2$  pulses (Fig. 6c). The pulse sequence decoupled the Ti spin from slow magnetic noises. As shown in Fig. 6c, the echo signal decays exponentially with pulse separation time, yielding a much longer coherence time of  $\sim 190$  ns. This indicates that one of the main decoherence sources of the Ti spin is the slow varying tip magnetic field, in addition to the tunneling current and scattering electrons from the tip and substrate[33].

By placing two Ti atoms close to each other using STM manipulations, one can demonstrate two-qubit gate operations [33]. Dipolar and exchange interaction between two Ti atoms in the spin-1/2 dimer produce a four-level energy spectrum (Fig. 6d), which can be

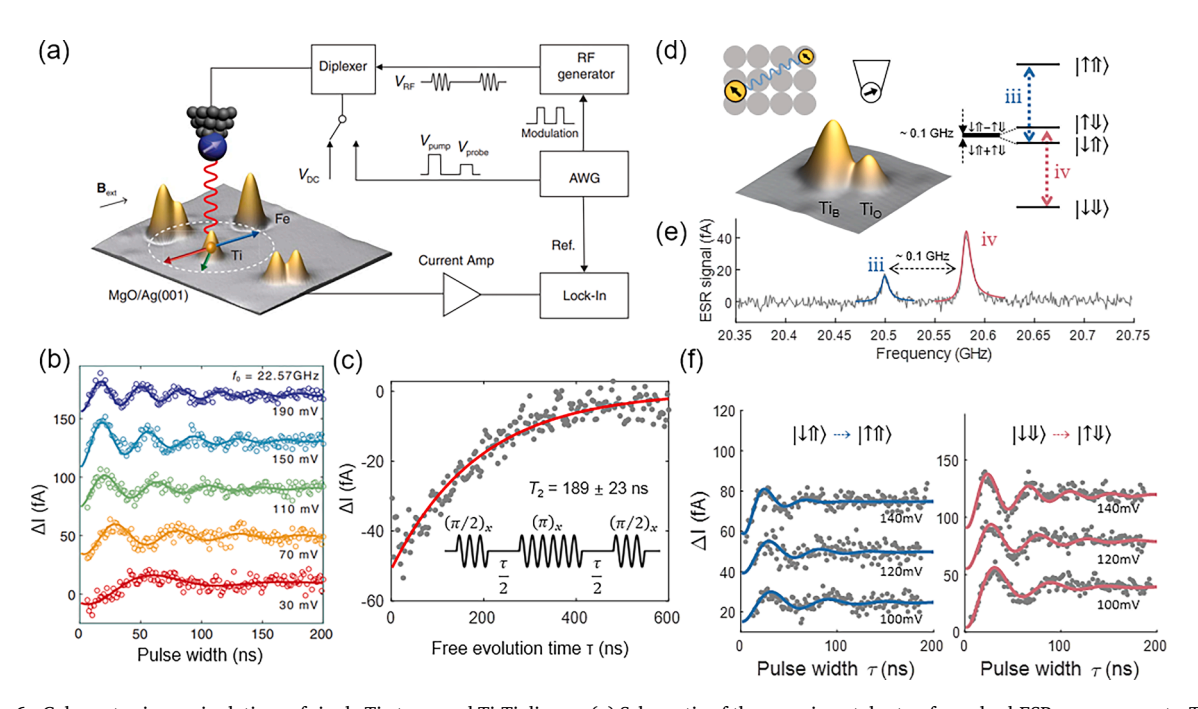


Fig. 6. Coherent spin manipulations of single Ti atoms and Ti-Ti dimers. (a) Schematic of the experimental setup for pulsed-ESR measurements. The RF and DC pulse sequences are applied on an Ti atom adsorbed on MgO/Ag(100). (b) Rabi oscillations of the Ti spin at different RF voltages. (c) Hahn-echo signals of the Ti spin, yielding a coherence time of  $\sim$  190 ns. (d) STM image and energy level diagram of one oxygen-site and one bridge-site Ti atom on MgO. (e) CW-ESR spectrum of the Ti-Ti dimer. The two peaks correspond to the transitions marked in the right panel of (d). (f) Pulsed-ESR measured on the oxygen-site Ti atom corresponding to the two transitions marked in the right panel of (d). Reprinted and adapted with permission from Ref. [33]. Copyright 2019 American Association for the Advancement of Science.

characterized by ESR-STM (Fig. 6e)[33,78]. The CW-ESR spectrum reveals two transitions, suggesting that spin-flipping of the target spin can be manipulated by selective microwaves. By setting the RF frequency to one of the ESR transitions, the RF pulse flipped the target spin (Ti atom under the tip) if and only if the control spin (nearby Ti atom) is in the spin-up or spin-down state, which can be regarded as a realization of a two-qubit CNOT gate (Fig. 6f). We note that Phark *et al.* recently reported the observation of electron–electron double resonance of two magnetically coupled Ti ( $S = \frac{1}{2}$ ) atoms[95]. With the tip positioned on just one of the two spins, either spin can be resonantly driven independently at its distinct resonant frequency by combining multiple RF signals into the tunneling junction. This could enable the remote sensing of the spin dynamics with ESR-STM and potentially avoid the decoherence due to the perturbation at the tunneling junction.

Coherent spin manipulations by pulsed-ESR can be extended to explore single molecular magnets on surfaces [34,92]. Compared to magnetic atoms, molecular magnets can be tailored by their ligand structure and a molecular network provides a way toward scalability. Using ESR-STM, Willke *et al.* demonstrated the coherent spin manipulation of single iron phthalocyanine (FePc) molecules on the surface of bilayer MgO (Fig. 7a) and showed that the spin decoherence is weakly influenced by the intermolecular magnetic coupling in molecules [34].

The FePc molecule on MgO was found to be a spin-1/2 anion system supported by DFT calculations and displays weakly anisotropic g-factors[92]. The fast spin dynamics of a single FePc spin can be accessed by measuring the Rabi oscillations at the center of the molecule (Fig. 7b)[34], which shows similar Rabi frequencies as well as the coherence time ( $\sim$ 40 ns) as the Ti atoms on MgO[33]. Hahn-echo measurements performed on single FePc yielded a maximum coherence time of  $\sim$  400 ns at a tunneling current of  $\sim$  0.8 pA [34]. This value is larger than that of the Ti atom on MgO measured at  $\sim$  3 pA due to the much lower tunneling current since a dominating decoherence channel for the surface spin is the scattering by electrons from the tunneling current.

In self-assembled FePc nanostructures, the random spin flip of a neighboring molecule could influence the spin coherence time of the FePc under the STM tip. To study this effect, FePc molecules with different numbers of neighbors were measured by ESR-STM[34]. The FePc molecules are weakly coupled and their eigenstates can be approximated by the Zeeman product states[78], with the corresponding ESR spectra shown in Fig. 7c. Fig. 7d shows the Hahn-echo signal for FePc with different numbers of neighbors, and it is found that the Hahn-echo coherence time only decreased slightly with increasing numbers of neighbors (Fig. 7e). This suggests the possibility of building larger FePc arrays without affecting the coherence time of individual molecular spins.

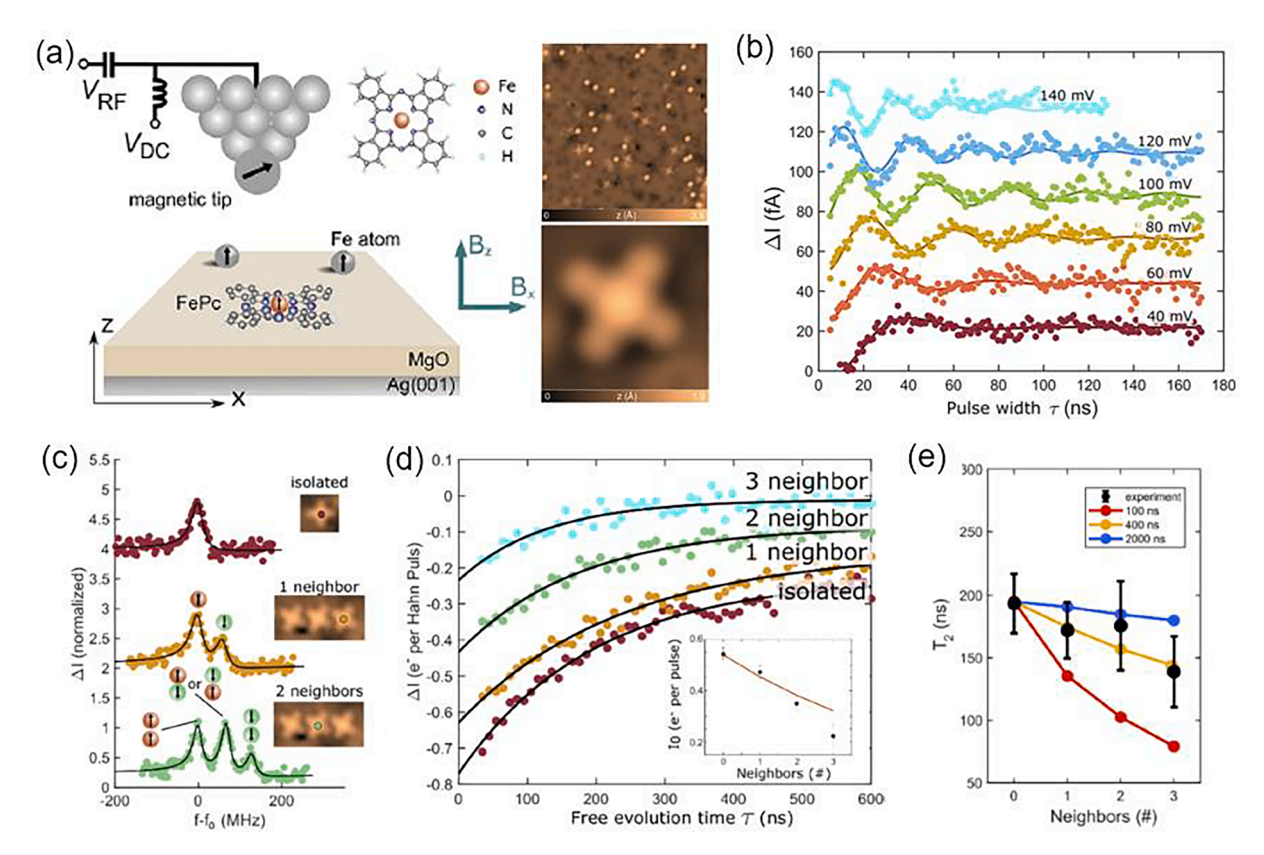


Fig. 7. Coherent spin manipulations of single FePc molecules. (a) Schematic of the experiment setup, the molecular configuration of FePc, and the STM image of FePc on MgO. (b) Rabi oscillations of the FePc spin at different RF voltages. (c) ESR spectra of FePc molecules with different number of neighbors. (d) Hahn-echo measurements on FePc with different numbers of neighbors. (e) Spin coherence time from Hahn-echo measurements and the simulation results for FePc with different numbers of neighbors. Reprinted with permission from Ref. [34]. Copyright 2021 American Chemical Society.

#### 3.5. Two-level system in a double-well potential

Besides the spin degree of freedom, other binary quantum levels may also serve as the building blocks of quantum devices. One inventive example is the hydrogen molecule in an asymmetric double-well potential. As discussed previously, the molecule in a double-well potential can switch between two conformational states. For a relatively heavy molecule such as MgPc or pyrrolidine, these two states are often well separated in the reaction coordinate. The transition between them requires the excitation into an intermediate state above the energy barrier, such as the ionized state for MgPc[27]. However, for a small molecule like hydrogen, quantum tunneling can occur[96–98]. The wavefunction spreads out in both potential wells resulting in a set of orthogonal bases |a> and |b> with an energy gap  $\Delta \varepsilon$  co-defined by inter barrier tunneling rate  $\Delta_0$  and the asymmetric energy of the two local minimum  $\varepsilon$  as  $\Delta \varepsilon=$ 

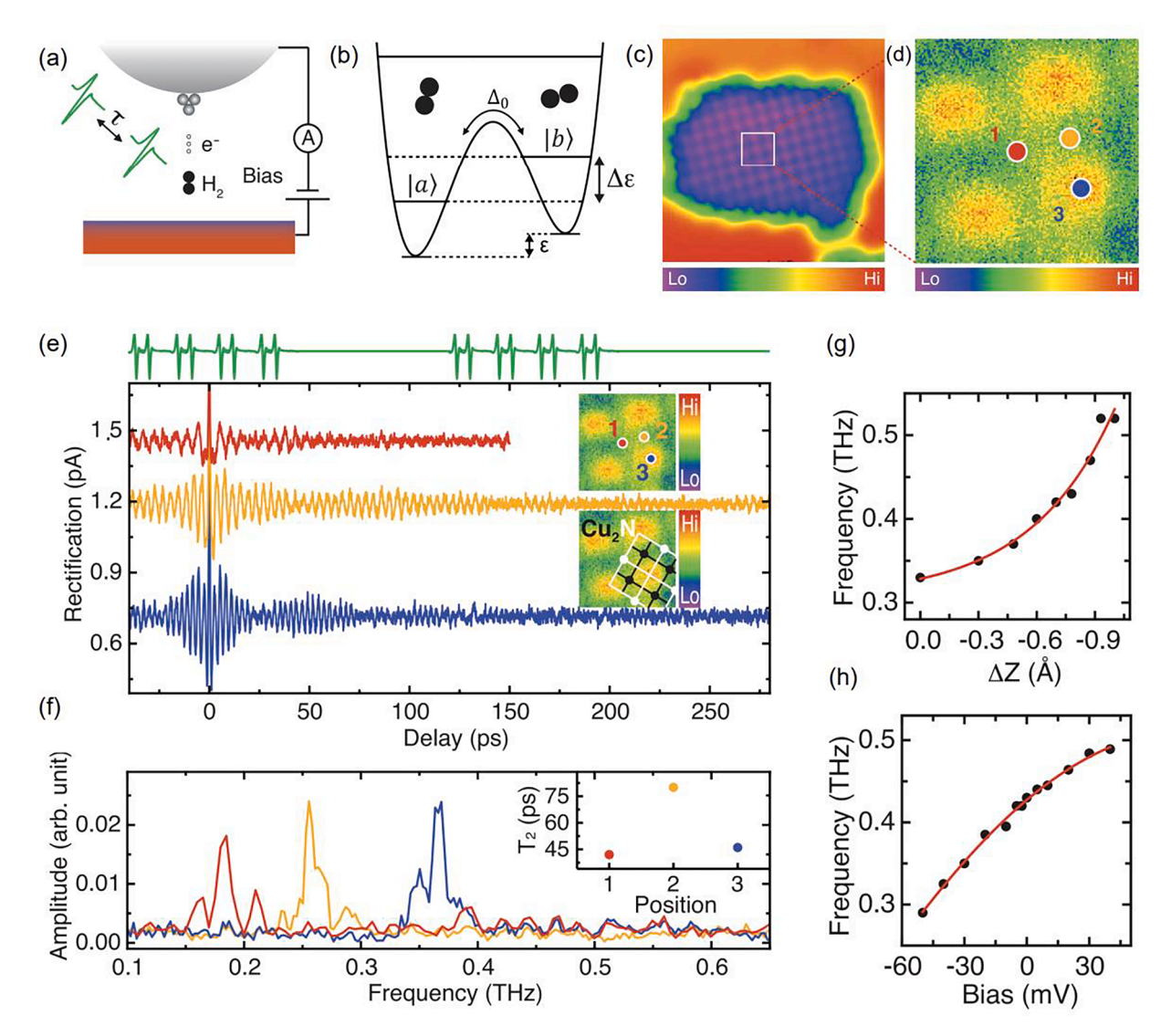


Fig. 8. Quantum sensing based on the coherent dynamics of the  $H_2$  in a tunnel junction. (a) Schematic of the  $H_2$  in an STM cavity illuminated by paired THz pulses. (b) Energy profile of two conformational states of  $H_2$ , |a> and |b>.  $\triangle \epsilon$ ,  $\Delta_0$  and  $\epsilon$  denote the energy gap between two states, the inter-barrier tunneling rate, and the asymmetric energy of the two local minimum, respectively. (c) Topographic image of a  $Cu_2N$  island. (d) Zoomin image of the area indicated in (c). The red, yellow and blue dots are over the hollow, bridge and top sites of the  $Cu_2N$  lattice respectively. (e) THz-induced rectification current as a function of the delay time between two identical pulses. The three spectra were acquired over the positions of corresponding colors in the top inset. The bottom inset shows the topographic image with  $Cu_2N$  lattice overlaid. (f) Fourier transform of the corresponding spectra in (e) unveil three distinct peaks. The inset shows the position-dependent decoherence time  $T_2$  which is extracted by fitting the spectra in (e). (g) Oscillation frequency of the THz-induced rectification current over the same position as a function of the tunneling gap. The red curve is an exponential fit. (h) Oscillation frequency as a function the DC bias. Reprinted and adapted with permission from Ref. [44]. Copyright 2022 American Association for the Advancement of Science. (For interpretation of the references to colour in this figure legend, the reader is referred to the web version of this article.)

 $\sqrt{\Delta_0^2 + \epsilon^2}$  [99]. Such a two-level system exists without an external magnetic field and thus can potentially realize quantum gates in a practical environment [100,101].

Very recently, Wang *et al.* fabricated a quantum sensor with a hydrogen molecule and used its spatial inhomogeneity in coherent dynamics to visualize the atomic-scale variation in potential landscape (Fig. 8a)[44]. In this experiment, the asymmetric double-well potential defined by the STM tip and the  $Cu_2N/Cu(1\,1\,0)$  substrate creates two quantum states, |a> and |b>, with a small  $\Delta\epsilon$  (Fig. 8b). Weak-field (4.2 mV peak voltage), and high-repetition (1 GHz) THz pulses are used in the pump–probe measurement to trace the

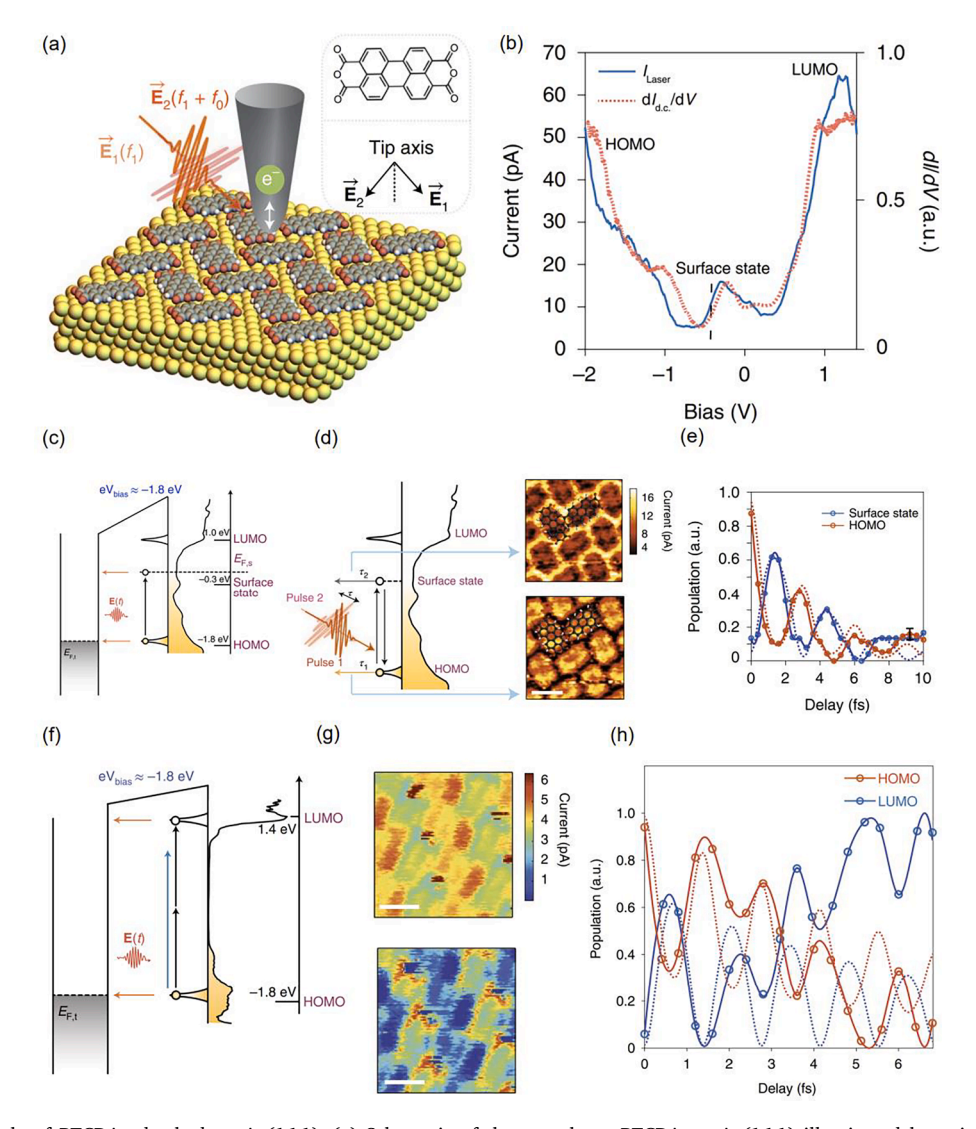


Fig. 9. Rabi cycle of PTCDA adsorbed on Au(111). (a) Schematic of the monolayer PTCDA on Au(111) illuminated by paired orthogonally polarized NIR laser pulses, which differ in carrier frequency by  $f_0$ . The top inset shows the structure of PTCDA while the bottom one demonstrates the relative direction between the electric field of the two pulses and the tip axis. (b) The dI/dV spectrum and laser-induced tunneling current over the monolayer PTCDA. (c) Schematic of the laser-induced electronic transition and tunneling at -1.8 V bias, where the HOMO of monolayer PTCDA and the Fermi surface of the tip are aligned. The Au surface state and the HOMO of PTCDA are dipole coupled by the photon. (d) Left panel: Illustration of the Rabi oscillation between the Au surface state and HOMO of PTCDA, which is detected in a pump–probe scheme. Right panels: The two spatial mappings of laser-induced current over the same area at two different delay time,  $\tau_1$  (0 fs) and  $\tau_2$  (1.2 fs), highlight the HOMO of PTCDA and Au surface state respectively. (e) The population of HOMO of PTCDA and Au surface state as a function of the delay time. The solid lines are experimental data while the dashed lines are fittings with a two-state model. (f) Schematic of the laser-induced electronic transition and tunneling at -1.8 V bias, where the HOMO of 4-layered PTCDA and the Fermi surface of the tip are aligned. The blue and black arrow lines are one- and two-photon processes, respectively. (g) Spatial mappings of the laser-induced current over the same area show the HOMO (top panel, 1.2 fs delay) and LUMO (bottom panel, 0.8 fs delay) of 4-layered PTCDA, respectively. (h) The population of HOMO and LUMO of 4-layered PTCDA as a function of the delay time. The solid lines are experimental data while the dashed lines are fittings with a two-state model. Reprinted with permission from Ref. [35]. Copyright 2021 Springer Nature. (For interpretation of the references to colour in this figure legend, the reader is referred to the web version of th

quantum coherence of  $H_2$ . The pump pulse excites the transition of  $H_2$  between |a> and |b> through a Rabi process. We note that this mechanism is different from the previous THz-STM measurements where the molecules are excited by electron tunneling driven by a much stronger THz field (Figs. 1-2)[26,27]. Here, the transition between two states is triggered by the absorption of THz photon in resonance with  $\Delta \epsilon$ . The probe pulse modulates the DC bias and induces a rectification current, which the authors showed to be proportional to the second derivative of the DC tunneling current at a given sample bias. The amplitude of the rectification current peaks correlates with a specific superposition of |a> and |b>. The time evolution of the rectification current exhibits a prominent oscillatory feature, which was assigned as the Ramsey interference. The measured oscillation frequency at the three nearby highsymmetry positions on the Cu<sub>2</sub>N island shows an obvious frequency shift up to 58 GHz/Å (Fig. 8c-f), even though the inelastic tunneling spectroscopy spectra acquired at these locations are indistinguishable. The authors attributed this frequency shift to a combined result of the spatial variation of the surface electric field and the change in the barrier height of the double-well potential. This mechanism was supported by the measured oscillation frequency shift in response to the DC bias as well as the tip-substrate separation. When the DC bias is increased at a fixed tip-substrate distance, the energy ε varies as a result of the Stark effect, leading to a change in the oscillation frequency (Fig. 8h). As the tip moves towards the substrate at a fixed bias, besides the increase of the electric field, the decrease of the barrier height leads to a higher tunneling rate  $\Delta_0$ , which further increases the oscillation frequency (Fig. 8g). Based on the measurement, the authors obtained a surface electrostatic field of 43 mV/Å pointing toward the surface and a ~ 0.6 Debye difference between the molecular dipoles in  $|a\rangle$  and  $|b\rangle$ . Apart from the dominant frequency, some satellite peaks resulting in the beating of the oscillation are routinely resolved (Fig. 8f), which was attributed to the degeneracy lift of the two-level system by the tip asymmetry or lattice mismatch between Cu<sub>2</sub>N and Cu(110). The decoherence time, another parameter directly related to the coupling with the local environment also shows obvious spatial inhomogeneity (Fig. 8f). This study again showcases that the quantum coherence of a two-level system is very sensitive to the atomic-scale local chemical environment.

#### 3.6. Rabi cycle of molecular electronic states

Another example of a two-level system is the superposition of binary electronic states of a surface-adsorbed molecule. Garg et al. studied the self-assembled mono/multi-layer perylene tetracarboxylic dianhydride (PTCDA) on Au(111) substrate and revealed the quantum coherence of the binary electronic system consisting of either the HOMO and LUMO of PTCDA or the PTCDA HOMO and a surface state of Au(111) (Fig. 9a)[35]. In the experiment, a W tip/PTCDA/Au(111) junction is illuminated with orthogonally polarized ultrashort (<6 fs) broadband (~0.36 eV FWHM) NIR laser pulses pairs centered at 810 nm. One of the paired pulses is shifted by a small frequency difference ( $f_0 \sim 800 \text{ Hz}$ ) with an acoustic-optic frequency shifter. The second-order effect-induced tunneling current oscillating at  $f_0$  can be detected with a lock-in amplifier. Since the pulse interval is  $\sim 11$  ns and shorter than the reported  $\sim 100$ ns thermal fluctuation timescale [36], the authors expected that the tunnel junction views the laser pulses as a constant thermal load and excluded the spurious signal from tip expansion and contraction. They kept the electric fields of the pump and probe pulses 45°/-45° away from the tip so that the components of the electric fields in the sample plane can couple the electronic states through dipole interaction. Given the selective enhancement of the electric field along the tip axis, there remains a concern that the orthogonality between the polarization of pump and probe pulses may be broken at the junction and hence the interference of the enhanced field parallel to the tip might contribute to the detected signal. The measured laser-induced tunneling current is proportional to the local density of states, indicating that the photon-populated electronic states, either molecular orbitals or Au surface state, are the main sources of the tunneling electrons at the corresponding bias (Fig. 9b). Nonetheless, the relatively large photo-induced current ( $\sim$ 10 pA) indicates that multiple electrons are excited by a single pulse, which is probably due to the hybridization among PTCDAs or with the Au substrate. Since the photon energy of the laser in use is  $\sim 1.5$  eV, the Au surface state ( $\sim -0.3$  eV) and the HOMO of the PTCDA ( $\sim -1.8$ eV) form a readily accessible two-level system by STM when the HOMO is aligned with the Fermi surface of the tip at -1.8 V sample bias (Fig. 9c). In the pump-probe measurement by applying a temporal delay between the two laser pulses, the authors mapped out the relative weight of the two states with joint space-time resolution and found the populations of Au surface state and HOMO of the PTCDA both oscillate with a period of ~ 2.7 fs but in the opposite phase (Fig. 9d-e). This oscillation frequency matches the energy difference (1.5 eV) between the two states. The decoherence occurs as fast as  $\sim 5$  fs which is extracted by fitting the time evolution of the measured laser-induced tunneling current with a decaying oscillation curve. The fast decoherence was attributed to the scattering with the underlying conduction electrons in the Au substrate. Rabi oscillation between the HOMO and LUMO of the PTCDA can also be observed on the molecular multi-layers where the top-layer molecules are effectively decoupled from the Au substrate. A  $\sim 1.4$  fs oscillation is measured over the 4-layered PTCDA and was assigned as the HOMO-LUMO transition which has a larger energy gap compared with the transition between HOMO and the Au surface state (Fig. 9f-h). However, it remains unclear why the measured population of LUMO increases with time, which was tentatively attributed to the competition between one- and two-photon processes. Although using molecular electronic states for quantum computation often faces a practical challenge: fast decoherence due to the strong interactions with bath, the molecular-scale engineering, and characterization of quantum electronic coherence could provide insights into how to prolong the lifetime of a molecular qubit by utilizing other degrees of freedom, such as the electron spin.

## 4. Summary and outlook

In this review, we have discussed the different means by which STM can integrate with electromagnetic excitation to investigate quantum coherent phenomena. Atomic-scale characterization of the time evolution of quantum states enables the direct visualization of the nature of quantum entanglement and superposition. Different wavelengths of electromagnetic sources including visible, infrared, THz, and microwave are used to drive or manipulate atomic or molecular coherence. A series of quantum coherent processes,

such as molecular vibration, electron transfer, localized surface plasmon, coherent phonon, electron spin resonance, and electronic excitation are investigated with joint space–time resolution. These coherent phenomena cover a wide timescale from hundreds of attoseconds to a few milliseconds. Different coupling effects between the atom or molecule and its chemical environment and their corresponding influence on the decoherence dynamics can be separately characterized. The realization or promise of coherent manipulation at a single molecule or atom level is demonstrated in some cases.

The THz-induced electron tunneling, perturbation to the local potential well, absorption of the infrared photon, or the stimulated Raman process can drive the vibration excitation of different molecules including pentacene, phthalocyanine, and pyrrolidine. The decoherence timescale depends sensitively on the substrates where the molecules adsorb, from hundreds of picoseconds on insulating substrates to sub-picosecond on metal surfaces. Other minor changes in the local chemical environment, such as the interaction between two adjacent molecules in a cluster, or the long-range van der Waals interaction, also altered the coherence dynamics of the molecule.

The highly enhanced and localized electric field generated at the STM tip apex under light illumination can also excite the collective motion of electrons or nuclei near the sample surface. The electron oscillation (surface plasmon) often decays within a few femto-seconds and serves as an intermediate step of photoexcitation. The nuclei motion (phonon), on the other hand, can be much longer lived and frequently acts as the decay channel of other excited states. Investigation of the coherent surface plasmons and phonons has provided insights into the generation and damping mechanism of many other quantum coherent phenomena.

The coherent vibration, phonon, and electron motion all represent the cross-correlation between a quantum state and an electromagnetic perturbation. They, from our point of view, do not target the entanglement of quantum states which is the essence of quantum coherence. The investigation of binary quantum systems, on the other hand, has revealed properties related to the superposition of two wavefunctions. A single hydrogen molecule trapped underneath the STM tip, the unpaired electron in an atom or molecule in an external magnetic field, or two electronic states of a surface-adsorbed PTCDA molecule, are all examples of two-level quantum systems. The resonant transition between the two levels occurs when the driving photon matches their energy difference. The quantum entanglement can be manipulated by, for example, the Rabi or Ramsey process. For the hydrogen molecule in a double well potential, the adsorption of THz photon drives its conformational switching between two local minimums. The energy profile of the double-well potential changes as the hydrogen molecule moves with the STM tip, leading to a spatial variation of the temporal oscillations and decoherence in the superposition state. This demonstrates the capability of using a single molecule as a quantum sensor to characterize the spatial inhomogeneity of the potential energy surface. Meanwhile, the discrete spin energy levels of magnetic atoms or molecules can host a relatively long decoherence time of hundreds of nanoseconds, and thus are promising candidates to realize qubit operations. The atomically confined magnetic interaction between the STM tip and surface can excite and modify the coherent spin rotations of individual atoms or molecules on a surface. The pulse durations, sequencing, and intensity of the driving microwave provide a series of tuning knobs to control the spin superposition, enabling a powerful suite of pulsed techniques for atomic-scale magnetic sensing and simulation of magnetism in artificial magnetic nanostructures. Moreover, the creation of entangled electronic states in surface-adsorbed PTCDA further shines a light on utilizing the discrete molecular energy levels to fabricate qubits,

Besides the abovementioned quantum coherent phenomena, there are still many unexplored territories. For example, circularly polarized light can be utilized to manipulate the spin state of conducting electrons in semiconductors[40], which we anticipate being extended into the surface-adsorbed atoms and molecules. This could potentially provide an all-optical approach to manipulating the spin molecular qubits. Moreover, the oscillating electric field in resonance with a two-level system can split the energy levels through the Autler-Townes effect, which has been reported in several systems[102–104], but not yet with STM. It would be interesting to study how such an effect influences a single atom or molecule as well as its response to the variation in the local chemical environment. Likewise, access to nuclear spin states can be readily obtained by directly measuring the nuclear hyperfine splitting using ESR-STM [91,105]. An attractive but challenging goal for ESR-STM experiments would be to coherently control the spin states of a nucleus, which could potentially be achieved by exploiting the nuclear hyperfine coupling to an unpaired electron and the relative ease with which ESR-STM can probe and manipulate electron spins. In the context of quantum information science, the benefits of atomic-scale access to nuclear spins are evident: nuclear spins generally have coherence times several orders of magnitude longer than electron spins.

In summary, combining pulsed electromagnetic excitation with atomic-scale characterization presents an unprecedented opportunity to explore coherent physics and chemistry at the space–time limit. The research work covered in this review has demonstrated the existence of a variety of coherent phenomena in atoms and molecules as well as the feasibility to characterize them with STM. These studies have provided insights into the connection between decoherence dynamics and local environments, which could guide the future design and application of practical quantum devices including qubits and quantum sensors. The measurements performed on single atoms and molecules are expandable to atomic or molecular networks where quantum coherence holds the potential to revolutionize communication efficiency. Although most of the existing studies are performed in extreme experimental conditions or on exotic materials, we are optimistic about the future expansion to various practical systems such as biological molecules [106–111]. The success of coherent manipulation in certain systems further shines a light on the atomic-level steering of the appropriate observable or wavefunction from an initial state to the desired destination. We expect additional coherent manipulation approaches, such as the pump-dump scheme in the time domain and the multi-photon interference in the frequency domain [10], will be soon integrated with STM, which will be impactful in a broad range of research fields from synthetic chemistry to quantum information science.

# **Declaration of Competing Interest**

The authors declare that they have no known competing financial interests or personal relationships that could have appeared to

Progress in Surface Science xxx (xxxx) xxx

L. Bi et al.

influence the work reported in this paper.

#### Acknowledgments

This research is supported by the National Science Foundation Grant DMR-2011924, UC San Diego Materials Research Science and Engineering Center (UCSD MRSEC). K. Y. acknowledges support from the National Natural Science Foundation of China (12174433) and the CAS Project for Young Scientists in Basic Research (YSBR-003).

#### References

- [1] G.D. Scholes, G.R. Fleming, L.X. Chen, A. Aspuru-Guzik, A. Buchleitner, D.F. Coker, G.S. Engel, R. van Grondelle, A. Ishizaki, D.M. Jonas, J.S. Lundeen, J. K. McCusker, S. Mukamel, J.P. Ogilvie, A. Olaya-Castro, M.A. Ratner, F.C. Spano, K.B. Whaley, X. Zhu, Using coherence to enhance function in chemical and biophysical systems, Nature 543 (2017) 647–656.
- [2] H.W. Rathbone, J.A. Davis, K.A. Michie, S.C. Goodchild, N.O. Robertson, P.M.G. Curmi, Coherent phenomena in photosynthetic light harvesting: part one-theory and spectroscopy, Biophys. Rev. 10 (2018) 1427–1441.
- [3] W.H. Miller, Perspective: Quantum or classical coherence? J. Chem. Phys. 136 (2012), 210901.
- [4] Y. Aharonov, E. Cohen, F. Colombo, T. Landsberger, I. Sabadini, D.C. Struppa, J. Tollaksen, Finally making sense of the double-slit experiment, Proc. Natl. Acad. Sci. 114 (2017) 6480–6485.
- [5] C.H. Kim, T. Joo, Coherent excited state intramolecular proton transfer probed by time-resolved fluorescence, PCCP 11 (2009) 10266-10269.
- [6] Y. Li, J. Wang, M.L. Clark, C.P. Kubiak, W. Xiong, Characterizing interstate vibrational coherent dynamics of surface adsorbed catalysts by fourth-order 3D SFG spectroscopy, Chem. Phys. Lett. 650 (2016) 1–6.
- [7] T.I.C. Jansen, S. Saito, J. Jeon, M. Cho, Theory of coherent two-dimensional vibrational spectroscopy, J. Chem. Phys. 150 (2019), 100901.
- [8] W. Min, C.W. Freudiger, S. Lu, X.S. Xie, Coherent nonlinear optical imaging: beyond fluorescence microscopy, Annu. Rev. Phys. Chem. 62 (2011) 507–530.
- [9] T. Rathje, A.M. Sayler, S. Zeng, P. Wustelt, H. Figger, B.D. Esry, G.G. Paulus, Coherent control at its most fundamental: carrier-envelope-phase-dependent electron localization in photodissociation of a H<sup>±</sup><sub>2</sub> molecular ion beam target, Phys. Rev. Lett. 111 (2013), 093002.
- [10] M. Shapiro, P. Brumer, Coherent control of molecular dynamics, Rep. Prog. Phys. 66 (2003) 859-942.
- [11] G.D. Scholes, Coherence from Light Harvesting to Chemistry, J. Phys. Chem. Lett. 9 (2018) 1568–1572.
- [12] K.E. Aidala, R.E. Parrott, T. Kramer, E.J. Heller, R.M. Westervelt, M.P. Hanson, A.C. Gossard, Imaging magnetic focusing of coherent electron waves, Nat. Phys. 3 (2007) 464–468.
- [13] P. Brumer, M. Shapiro, Coherence chemistry: controlling chemical reactions [with lasers], Acc. Chem. Res. 22 (1989) 407-413.
- [14] H. Rabitz, R. de Vivie-Riedle, M. Motzkus, K. Kompa, Whither the future of controlling quantum phenomena? Science 288 (2000) 824.
- [15] R.J. Gordon, L. Zhu, T. Seideman, Coherent control of chemical reactions, Acc. Chem. Res. 32 (1999) 1007-1016.
- [16] M.B. Plenio, Coherence as a Resource An Overview, in: Rochester Conference on Coherence and Quantum Optics (CQO-11), Optica Publishing Group, Rochester, New York, 2019, p. pp. M2A.1.
- [17] F. Lombardi, A. Lodi, J. Ma, J. Liu, M. Slota, A. Narita, W.K. Myers, K. Müllen, X. Feng, L. Bogani, Quantum units from the topological engineering of molecular graphenoids, Science 366 (2019) 1107–1110.
- [18] A. Gaita-Ariño, F. Luis, S. Hill, E. Coronado, Molecular spins for quantum computation, Nat. Chem. 11 (2019) 301–309.
- [19] R.H. Lavroff, D.L. Pennington, A.S. Hua, B.Y. Li, J.A. Williams, A.N. Alexandrova, Recent Innovations in Solid-State and Molecular Qubits for Quantum Information Applications, J. Phys. Chem. Lett. 12 (2021) 10742–10745.
- [20] S. von Kugelgen, D.E. Freedman, A chemical path to quantum information, Science 366 (2019) 1070–1071.
- [21] A.P. Hines, P.C.E. Stamp, Decoherence in quantum walks and quantum computers, Can. J. Phys. 86 (2008) 541–548.
- [22] G. Binnig, H. Rohrer, C. Gerber, E. Weibel, Surface studies by scanning tunneling microscopy, Phys. Rev. Lett. 49 (1982) 57–61.
- [23] J.F. Schultz, S. Li, S. Jiang, N. Jiang, Optical scanning tunneling microscopy based chemical imaging and spectroscopy, J. Phys. Condens. Matter 32 (2020), 463001
- [24] Y.E. Tian, F.A.N. Yang, C. Guo, Y. Jiang, Recent advances in ultrafast time-resolved scanning tunneling microscopy, Surf. Rev. Lett. 25 (2018) 1841003.
- [25] R. Gutzler, M. Garg, C.R. Ast, K. Kuhnke, K. Kern, Light-matter interaction at atomic scales, Nat. Rev. Phys. 3 (2021) 441-453.
- [26] T.L. Cocker, D. Peller, P. Yu, J. Repp, R. Huber, Tracking the ultrafast motion of a single molecule by femtosecond orbital imaging, Nature 539 (2016) 263–267.
- [27] D. Peller, L.Z. Kastner, T. Buchner, C. Roelcke, F. Albrecht, N. Moll, R. Huber, J. Repp, Sub-cycle atomic-scale forces coherently control a single-molecule switch, Nature 585 (2020) 58–62.
- [28] S. Li, S. Chen, J. Li, R. Wu, W. Ho, Joint space-time coherent vibration driven conformational transitions in a single molecule, Phys. Rev. Lett. 119 (2017), 176002.
- [29] K. Yoshioka, I. Katayama, Y. Minami, M. Kitajima, S. Yoshida, H. Shigekawa, J. Takeda, Real-space coherent manipulation of electrons in a single tunnel junction by single-cycle terahertz electric fields, Nat. Photonics 10 (2016) 762–765.
- [30] M. Garg, K. Kern, Attosecond coherent manipulation of electrons in tunneling microscopy, Science (2019) eaaz1098.
- [31] S. Sheng, A.-C. Oeter, M. Abdo, K. Lichtenberg, M. Hentschel, S. Loth, Launching Coherent Acoustic Phonon Wave Packets with Local Femtosecond Coulomb Forces, Phys. Rev. Lett. 129 (2022), 043001.
- [32] S. Liu, A. Hammud, I. Hamada, M. Wolf, M. Müller, T. Kumagai, Nanoscale coherent phonon spectroscopy, Sci. Adv. 8 (2022) eabq5682.
- [33] K. Yang, W. Paul, S.-H. Phark, P. Willke, Y. Bae, T. Choi, T. Esat, A. Ardavan, A.J. Heinrich, C.P. Lutz, Coherent spin manipulation of individual atoms on a surface. Science 366 (2019) 509.
- [34] P. Willke, T. Bilgeri, X. Zhang, Y. Wang, C. Wolf, H. Aubin, A. Heinrich, T. Choi, Coherent Spin Control of Single Molecules on a Surface, ACS Nano 15 (2021) 17959–17965.
- [35] M. Garg, A. Martin-Jimenez, M. Pisarra, Y. Luo, F. Martín, K. Kern, Real-space subfemtosecond imaging of quantum electronic coherences in molecules, Nat. Photonics 16 (2022) 196–202.
- [36] C. Guo, X. Meng, H. Fu, Q. Wang, H. Wang, Y. Tian, J. Peng, R. Ma, Y. Weng, S. Meng, E. Wang, Y. Jiang, Probing nonequilibrium dynamics of photoexcited polarons on a metal-oxide surface with atomic precision, Phys. Rev. Lett. 124 (2020), 206801.
- [37] Y. Terada, S. Yoshida, O. Takeuchi, H. Shigekawa, Real-space imaging of transient carrier dynamics by nanoscale pump-probe microscopy, Nat. Photonics 4 (2010) 869–874.
- [38] S.W. Wu, W. Ho, Two-photon-induced hot-electron transfer to a single molecule in a scanning tunneling microscope, Phys. Rev. B 82 (2010), 085444.
- [39] M. Garg, A. Martin-Jimenez, Y. Luo, K. Kern, Ultrafast Photon-Induced Tunneling Microscopy, ACS Nano 15 (2021) 18071–18084.
- [40] S. Yoshida, Y. Aizawa, Z.-H. Wang, R. Oshima, Y. Mera, E. Matsuyama, H. Oigawa, O. Takeuchi, H. Shigekawa, Probing ultrafast spin dynamics with optical pump-probe scanning tunnelling microscopy, Nat. Nanotechnol. 9 (2014) 588–593.
- [41] S. Yoshida, Y. Arashida, H. Hirori, T. Tachizaki, A. Taninaka, H. Ueno, O. Takeuchi, H. Shigekawa, Terahertz Scanning Tunneling Microscopy for Visualizing Ultrafast Electron Motion in Nanoscale Potential Variations, ACS Photonics 8 (2021) 315–323.
- [42] T.L. Cocker, V. Jelic, M. Gupta, S.J. Molesky, J.A.J. Burgess, G.D.L. Reyes, L.V. Titova, Y.Y. Tsui, M.R. Freeman, F.A. Hegmann, An ultrafast terahertz scanning tunnelling microscope, Nat. Photonics 7 (2013) 620–625.

- [43] V. Jelic, K. Iwaszczuk, P.H. Nguyen, C. Rathje, G.J. Hornig, H.M. Sharum, J.R. Hoffman, M.R. Freeman, F.A. Hegmann, Ultrafast terahertz control of extreme tunnel currents through single atoms on a silicon surface, Nat. Phys. 13 (2017) 591–598.
- [44] L. Wang, Y. Xia, W. Ho, Atomic-scale quantum sensing based on the ultrafast coherence of an H2 molecule in an STM cavity, Science 376 (2022) 401-405.
- [45] F. Huber, F.J. Giessibl, Low noise current preamplifier for qPlus sensor deflection signal detection in atomic force microscopy at room and low temperatures, Rev. Sci. Instrum. 88 (2017), 073702.
- [46] R. Huber, M. Koch, J. Feldmann, Laser-induced thermal expansion of a scanning tunneling microscope tip measured with an atomic force microscope cantilever, Appl. Phys. Lett. 73 (1998) 2521–2523.
- [47] V. Gerstner, A. Thon, W. Pfeiffer, Thermal effects in pulsed laser assisted scanning tunneling microscopy, J. Appl. Phys. 87 (2000) 2574-2580.
- [48] T. Tachizaki, K. Hayashi, Y. Kanemitsu, H. Hirori, On the progress of ultrafast time-resolved THz scanning tunneling microscopy, APL Mater. 9 (2021), 060903.
- [49] K. Kimura, Y. Morinaga, H. Imada, I. Katayama, K. Asakawa, K. Yoshioka, Y. Kim, J. Takeda, Terahertz-Field-Driven Scanning Tunneling Luminescence Spectroscopy, ACS Photonics 8 (2021) 982–987.
- [50] M. Abdo, S. Sheng, S. Rolf-Pissarczyk, L. Arnhold, J.A.J. Burgess, M. Isobe, L. Malavolti, S. Loth, Variable Repetition Rate THz Source for Ultrafast Scanning Tunneling Microscopy, ACS Photonics 8 (2021) 702–708.
- [51] Y. Luo, V. Jelic, G. Chen, P.H. Nguyen, Y.-J.-R. Liu, J.A.M. Calzada, D.J. Mildenberger, F.A. Hegmann, Nanoscale terahertz STM imaging of a metal surface, Phys. Rev. B 102 (2020), 205417.
- [52] S.E. Ammerman, V. Jelic, Y. Wei, V.N. Breslin, M. Hassan, N. Everett, S. Lee, Q. Sun, C.A. Pignedoli, P. Ruffieux, R. Fasel, T.L. Cocker, Lightwave-driven scanning tunnelling spectroscopy of atomically precise graphene nanoribbons, Nat. Commun. 12 (2021) 6794.
- [53] S. Yoshida, H. Hirori, T. Tachizaki, K. Yoshioka, Y. Arashida, Z.-H. Wang, Y. Sanari, O. Takeuchi, Y. Kanemitsu, H. Shigekawa, Subcycle Transient Scanning Tunneling Spectroscopy with Visualization of Enhanced Terahertz Near Field, ACS Photonics 6 (2019) 1356–1364.
- [54] T. Kang, Y.-M. Bahk, D.-S. Kim, Terahertz quantum plasmonics at nanoscales and angstrom scales, Nanophotonics 9 (2020) 435-451.
- [55] K. Yoshioka, I. Katayama, Y. Arashida, A. Ban, Y. Kawada, K. Konishi, H. Takahashi, J. Takeda, Tailoring Single-Cycle Near Field in a Tunnel Junction with Carrier-Envelope Phase-Controlled Terahertz Electric Fields, Nano Lett. 18 (2018) 5198–5204.
- [56] J.A. Fülöp, L. Pálfalvi, G. Almási, J. Hebling, High energy THz pulse generation by tilted pulse front excitation and Its nonlinear optical applications, J. Infrared, Millimeter, Terahertz Waves 32 (2011) 553–561.
- [57] J. Hebling, K.-L. Yeh, M.C. Hoffmann, B. Bartal, K.A. Nelson, Generation of high-power terahertz pulses by tilted-pulse-front excitation and their application possibilities, J. Opt. Soc. Am. B 25 (2008) B6–B19.
- [58] M.C. Hoffmann, K.-L. Yeh, J. Hebling, K.A. Nelson, Efficient terahertz generation by optical rectification at 1035 nm, Opt. Express 15 (2007) 11706-11713.
- [59] E.T. Papaioannou, R. Beigang, THz spintronic emitters: a review on achievements and future challenges, Nanophotonics 10 (2021) 1243-1257.
- [60] T. Seifert, S. Jaiswal, U. Martens, J. Hannegan, L. Braun, P. Maldonado, F. Freimuth, A. Kronenberg, J. Henrizi, I. Radu, E. Beaurepaire, Y. Mokrousov, P. M. Oppeneer, M. Jourdan, G. Jakob, D. Turchinovich, L.M. Hayden, M. Wolf, M. Münzenberg, M. Kläui, T. Kampfrath, Efficient metallic spintronic emitters of ultrabroadband terahertz radiation, Nat. Photonics 10 (2016) 483–488.
- [61] C.W. Berry, N. Wang, M.R. Hashemi, M. Unlu, M. Jarrahi, Significant performance enhancement in photoconductive terahertz optoelectronics by incorporating plasmonic contact electrodes, Nat. Commun. 4 (2013) 1622.
- [62] C.W. Berry, M. Jarrahi, Terahertz generation using plasmonic photoconductive gratings, New J. Phys. 14 (2012), 105029.
- [63] B. Langdon, J. Garlick, X. Ren, D.J. Wilson, A.M. Summers, S. Zigo, M.F. Kling, S. Lei, C.G. Elles, E. Wells, E.D. Poliakoff, K.D. Carnes, V. Kumarappan, I. Ben-Itzhak, C.A. Trallero-Herrero, Carrier-envelope-phase stabilized terawatt class laser at 1 kHz with a wavelength tunable option, Opt. Express 23 (2015) 4563-4572
- [64] B.E. Schmidt, A.D. Shiner, P. Lassonde, J.-C. Kieffer, P.B. Corkum, D.M. Villeneuve, F. Légaré, CEP stable 1.6 cycle laser pulses at 1.8 μm, Opt. Express 19 (2011) 6858–6864.
- [65] A. Alismail, H. Wang, G. Barbiero, N. Altwaijry, S.A. Hussain, V. Pervak, W. Schweinberger, A.M. Azzeer, F. Krausz, H. Fattahi, Multi-octave, CEP-stable source for high-energy field synthesis, Sci. Adv. 6 (2020).
- [66] S. Baumann, W. Paul, T. Choi, C.P. Lutz, A. Ardavan, A.J. Heinrich, Electron paramagnetic resonance of individual atoms on a surface, Science 350 (2015) 417–420.
- [67] P. Willke, W. Paul, F.D. Natterer, K. Yang, Y. Bae, T. Choi, J. Fernández-Rossier, A.J. Heinrich, C.P. Lutz, Probing quantum coherence in single-atom electron spin resonance, Sci. Adv. 4 (2018).
- [68] Y. Bae, K. Yang, P. Willke, T. Choi, A.J. Heinrich, C.P. Lutz, Enhanced quantum coherence in exchange coupled spins via singlet-triplet transitions, Sci. Adv. 4 (2018).
- [69] W. Paul, S. Baumann, C.P. Lutz, A.J. Heinrich, Generation of constant-amplitude radio-frequency sweeps at a tunnel junction for spin resonance STM, Rev. Sci. Instrum. 87 (2016), 074703.
- [70] J.L. Lado, A. Ferrón, J. Fernández-Rossier, Exchange mechanism for electron paramagnetic resonance of individual adatoms, Phys. Rev. B 96 (2017), 205420.
- [71] K. Yang, W. Paul, F.D. Natterer, J.L. Lado, Y. Bae, P. Willke, T. Choi, A. Ferrón, J. Fernández-Rossier, A.J. Heinrich, C.P. Lutz, Tuning the Exchange Bias on a Single Atom from 1 mT to 10 T, Phys. Rev. Lett. 122 (2019), 227203.
- [72] A.M. Shakirov, A.N. Rubtsov, P. Ribeiro, Spin transfer torque induced paramagnetic resonance, Phys. Rev. B 99 (2019), 054434.
- [73] J. Reina Gálvez, C. Wolf, F. Delgado, N. Lorente, Cotunneling mechanism for all-electrical electron spin resonance of single adsorbed atoms, Phys. Rev. B 100 (2019), 035411.
- [74] T.S. Seifert, S. Kovarik, C. Nistor, L. Persichetti, S. Stepanow, P. Gambardella, Single-atom electron paramagnetic resonance in a scanning tunneling microscope driven by a radio-frequency antenna at 4 K, Phys. Rev. Res., 2 (2020) 013032.
- [75] K. Yang, A. Heinrich, C. Lutz, Single-Atom Spin Resonance in a Scanning Tunneling Microscope, Chin. J. Vac. Sci. Tech 41 (2021) 897–912.
- [76] T.S. Seifert, S. Kovarik, D.M. Juraschek, N.A. Spaldin, P. Gambardella, S. Stepanow, Longitudinal and transverse electron paramagnetic resonance in a scanning tunneling microscope, Sci. Adv. 6 (2020).
- [77] Y. Chen, Y. Bae, A.J. Heinrich, Harnessing the Quantum Behavior of Spins on Surfaces, Adv. Mater., n/a (2022) 2107534.
- [78] T. Choi, W. Paul, S. Rolf-Pissarczyk, A.J. Macdonald, F.D. Natterer, K. Yang, P. Willke, C.P. Lutz, A.J. Heinrich, Atomic-scale sensing of the magnetic dipolar field from single atoms, Nat. Nanotechnol. 12 (2017) 420–424.
- [79] K. Yang, S.-H. Phark, Y. Bae, T. Esat, P. Willke, A. Ardavan, A.J. Heinrich, C.P. Lutz, Probing resonating valence bond states in artificial quantum magnets, Nat. Commun. 12 (2021) 993.
- [80] R. Drost, M. Uhl, P. Kot, J. Siebrecht, A. Schmid, J. Merkt, S. Wünsch, M. Siegel, O. Kieler, R. Kleiner, C.R. Ast, Combining electron spin resonance spectroscopy with scanning tunneling microscopy at high magnetic fields, Rev. Sci. Instrum. 93 (2022), 043705.
- [81] S. Loth, M. Etzkorn, C.P. Lutz, D.M. Eigler, A.J. Heinrich, Measurement of Fast Electron Spin Relaxation Times with Atomic Resolution, Science 329 (2010) 1628–1630.
- [82] S. Yan, D.-J. Choi, J.A.J. Burgess, S. Rolf-Pissarczyk, S. Loth, Control of quantum magnets by atomic exchange bias, Nat. Nanotechnol. 10 (2015) 40–45.
- [83] W. Paul, K. Yang, S. Baumann, N. Romming, T. Choi, C.P. Lutz, A.J. Heinrich, Control of the millisecond spin lifetime of an electrically probed atom, Nat. Phys. 13 (2017) 403–407.
- [84] L.M. Veldman, L. Farinacci, R. Rejali, R. Broekhoven, J. Gobeil, D. Coffey, M. Ternes, A.F. Otte, Free coherent evolution of a coupled atomic spin system initialized by electron scattering, Science 372 (2021) 964–968.
- [85] S. Kanai, F.J. Heremans, H. Seo, G. Wolfowicz, C.P. Anderson, S.E. Sullivan, M. Onizhuk, G. Galli, D.D. Awschalom, H. Ohno, Generalized scaling of spin qubit coherence in over 12,000 host materials, Proc. Natl. Acad. Sci. 119 (2022).
- [86] Ö. Bozat, Z. Gedik, Spin bath decoherence mediated by phonons, Solid State Commun. 148 (2008) 237-239.
- [87] C.C. Moser, C.C. Page, R.J. Cogdell, J. Barber, C.A. Wraight, P.L. Dutton, Length, time, and energy scales of photosystems, in: Advances in Protein Chemistry, Academic Press, 2003, pp. 71–109.

- [88] B. Giese, Long-Distance Electron Transfer Through DNA, Annu. Rev. Biochem 71 (2002) 51-70.
- [89] D.-J. Choi, N. Lorente, J. Wiebe, K. von Bergmann, A.F. Otte, A.J. Heinrich, Colloquium: Atomic spin chains on surfaces, Rev. Mod. Phys. 91 (2019), 041001.
- [90] A.A. Khajetoorians, D. Wegner, A.F. Otte, I. Swart, Creating designer quantum states of matter atom-by-atom, Nat. Rev. Phys. 1 (2019) 703-715.
- [91] P. Willke, Y. Bae, K. Yang, J.L. Lado, A. Ferrón, T. Choi, A. Ardavan, J. Fernández-Rossier, A.J. Heinrich, C.P. Lutz, Hyperfine interaction of individual atoms on a surface. Science 362 (2018) 336–339.
- [92] X. Zhang, C. Wolf, Y. Wang, H. Aubin, T. Bilgeri, P. Willke, A.J. Heinrich, T. Choi, Electron spin resonance of single iron phthalocyanine molecules and role of their non-localized spins in magnetic interactions. Nat. Chem. 14 (2022) 59–65.
- [93] M. Steinbrecher, W.M.J. van Weerdenburg, E.F. Walraven, N.P.E. van Mullekom, J.W. Gerritsen, F.D. Natterer, D.I. Badrtdinov, A.N. Rudenko, V. V. Mazurenko, M.I. Katsnelson, A. van der Avoird, G.C. Groenenboom, A.A. Khajetoorians, Quantifying the interplay between fine structure and geometry of an individual molecule on a surface, Phys. Rev. B 103 (2021), 155405.
- [94] F.D. Natterer, K. Yang, W. Paul, P. Willke, T. Choi, T. Greber, A.J. Heinrich, C.P. Lutz, Reading and writing single-atom magnets, Nature 543 (2017) 226–228.
- [95] S.-H. Phark, Y. Chen, C. Wolf, H.T. Bui, Y. Wang, M. Haze, J. Kim, C.P. Lutz, A.J. Heinrich, Y.J.a.p.a. Bae, Double Electron Spin Resonance of Engineered Atomic Structures on a Surface, (2021).
- [96] P. Esquinazi, Tunneling systems in amorphous and crystalline solids, Springer Science & Business Media, 2013.
- [97] L.J. Lauhon, W. Ho, Direct Observation of the Quantum Tunneling of Single Hydrogen Atoms with a Scanning Tunneling Microscope, Phys. Rev. Lett. 85 (2000) 4566–4569.
- [98] X. Meng, J. Guo, J. Peng, J. Chen, Z. Wang, J.-R. Shi, X.-Z. Li, E.-G. Wang, Y. Jiang, Direct visualization of concerted proton tunnelling in a water nanocluster, Nat. Phys. 11 (2015) 235–239.
- [99] C. Müller, J.H. Cole, J. Lisenfeld, Towards understanding two-level-systems in amorphous solids: insights from quantum circuits, Rep. Prog. Phys. 82 (2019), 124501.
- [100] B. Vaucher, A. Nunnenkamp, D. Jaksch, Creation of resilient entangled states and a resource for measurement-based quantum computation with optical superlattices, New J. Phys. 10 (2008), 023005.
- [101] V. Jelic, F. Marsiglio, The double-well potential in quantum mechanics: a simple, numerically exact formulation, Eur. J. Phys. 33 (2012) 1651-1666.
- [102] M. Reutzel, A. Li, Z. Wang, H. Petek, Coherent multidimensional photoelectron spectroscopy of ultrafast quasiparticle dressing by light, Nat. Commun. 11 (2020) 2230.
- [103] K.C. Miao, J.P. Blanton, C.P. Anderson, A. Bourassa, A.L. Crook, G. Wolfowicz, H. Abe, T. Ohshima, D.D. Awschalom, Universal coherence protection in a solid-state spin qubit, Science 369 (2020) 1493–1497.
- [104] S. Nandi, E. Olofsson, M. Bertolino, S. Carlström, F. Zapata, D. Busto, C. Callegari, M. Di Fraia, P. Eng-Johnsson, R. Feifel, G. Gallician, M. Gisselbrecht, S. Maclot, L. Neoričić, J. Peschel, O. Plekan, K.C. Prince, R.J. Squibb, S. Zhong, P.V. Demekhin, M. Meyer, C. Miron, L. Badano, M.B. Danailov, L. Giannessi, M. Manfredda, F. Sottocorona, M. Zangrando, J.M. Dahlström, Observation of Rabi dynamics with a short-wavelength free-electron laser, Nature 608 (2022) 488–493
- [105] J. Kim, K. Noh, Y. Chen, F. Donati, A.J. Heinrich, C. Wolf, Y. Bae, Anisotropic Hyperfine Interaction of Surface-Adsorbed Single Atoms, Nano Lett. (2022).
- [106] K. Michaeli, D.N. Beratan, D.H. Waldeck, R. Naaman, Voltage-induced long-range coherent electron transfer through organic molecules, Proceed. Natl. Acad. Sci., 116 (2019) 5931-5936.
- [107] Z. Futera, I. Ide, B. Kayser, K. Garg, X. Jiang, J.H. van Wonderen, J.N. Butt, H. Ishii, I. Pecht, M. Sheves, D. Cahen, J. Blumberger, Coherent Electron Transport across a 3 nm Bioelectronic Junction Made of Multi-Heme Proteins, J. Phys. Chem. Lett. 11 (2020) 9766–9774.
- [108] C. Andrea Rozzi, S. Maria Falke, N. Spallanzani, A. Rubio, E. Molinari, D. Brida, M. Maiuri, G. Cerullo, H. Schramm, J. Christoffers, C. Lienau, Quantum coherence controls the charge separation in a prototypical artificial light-harvesting system, Nat. Commun. 4 (2013) 1602.
- [109] G.S. Engel, T.R. Calhoun, E.L. Read, T.-K. Ahn, T. Mančal, Y.-C. Cheng, R.E. Blankenship, G.R. Fleming, Evidence for wavelike energy transfer through quantum coherence in photosynthetic systems, Nature 446 (2007) 782–786.
- [110] E. Collini, G.D. Scholes, Coherent Intrachain Energy Migration in a Conjugated Polymer at Room Temperature, Science 323 (2009) 369–373.
- [111] E. Collini, C.Y. Wong, K.E. Wilk, P.M.G. Curmi, P. Brumer, G.D. Scholes, Coherently wired light-harvesting in photosynthetic marine algae at ambient temperature, Nature 463 (2010) 644–647.